DOI: 10.1002/chem.200801454

Control of H- and J-Type π Stacking by Peripheral Alkyl Chains and Self-Sorting Phenomena in Perylene Bisimide Homo- and Heteroaggregates

Suhrit Ghosh, Xue-Qing Li, Vladimir Stepanenko, and Frank Würthner*[a]

Abstract: The synthesis, self-assembly, and gelation ability of a series of organogelators based on perylene bisimide (PBI) dyes containing amide groups at imide positions are reported. The synergetic effect of intermolecular hydrogen bonding among the amide functionalities and π–π stacking between the PBI units directs the formation of the self-assembled structure in solution, which beyond a certain concentration results in gelation. Effects of different peripheral alkyl substituents on the self-assembly were studied by solvent- and temperature-dependent UV-visible and circular dichroism (CD) spectroscopy. PBI derivatives containing linear alkyl side chains in the periphery formed H-type π stacks and red gels, whereas by introducing branched alkyl chains the formation of J-type π stacks and green gels could be achieved. Sterically demanding substituents, in particular, the 2-ethylhexyl group completely suppressed the π stacking. Coaggregation studies with H- and J-aggregating chromophores revealed the formation of solely H-type π stacks containing both precursor molecules at a lower mole fraction of J-aggregating chromophore. Beyond a critical composition of the two chromophores, mixed H-aggregate and J-aggregate were formed simultaneously, which points to a self-sorting process. The versatility of the gelators is strongly dependent on the length and nature of the peripheral alkyl substituents. CD spectroscopic studies revealed a preferential helicity of the aggregates of PBI building blocks bearing chiral side chains. Even for achiral PBI derivatives, the utilization of chiral solvents such as (*R*)- or (*S*)-limonene was effective in preferential population of one-handed helical fibers. AFM studies revealed the formation of helical fibers from all the present PBI gelators, irrespective of the presence of chiral or achiral side chains. Furthermore, vortex flow was found to be effective in macroscopic orientation of the aggregates as evidenced from the origin of CD signals from aggregates of achiral PBI molecules.

Keywords: dyes/pigments · organogelators · self-assembly · systems chemistry · vortex effect

Introduction

Supramolecular chemistry has come to the fore as an extensively studied research area in the recent past due to its implications in biology and materials science.[1] Self-organization of small molecular entities into well-defined supramolecular architectures is involved in various vital biological functions in living systems.[2] For example, organization of lipids in the form of bilayers within the cell membrane is necessary for life. Over the past decade, several noncovalent interactions such as hydrogen bonding, metal-ion-to-ligand coordination, electrostatic interactions, π–π stacking, dipole–dipole interactions, hydrophobic interactions, and so forth, have been identified as enabling the construction of various superstructures from specifically engineered small-molecule building blocks. Incorporation of building blocks bearing specific functionality[3] into larger entities has enormous potential for materials science due to the possibility of bridging the gap between the molecular scale and the macroscopic one in terms of structural order, when precise control of such a self-assembly process is achieved. Efforts have been made to create well-ordered supramolecular structures based on functional dye molecules[4] to expand their utilities in various organic electronic device applications. It is well understood that in many of the optical devices the efficient transport of charge carriers is essential for improved device performance. For example, in a bulk heterojunction solar cell, when charge-separated states are generated upon illumination, it is desirable that holes and electrons find the

[a] Dr. S. Ghosh, X.-Q. Li, V. Stepanenko, Prof. Dr. F. Würthner
Universität Würzburg
Institut für Organische Chemie and
Röntgen Research Center for Complex Material Systems
Am Hubland, 97074 Würzburg (Germany)
Fax: (+49) 931-888-4756
E-mail: wuerthner@chemie.uni-wuerzburg.de

Supporting information for this article is available on the WWW under http://dx.doi.org/10.1002/chem.200801454.

continuous pathway to the respective electrodes prior to recombination. Thus, higher ordering of p- and n-type semiconductors based on π-conjugated systems is necessary for enhanced charge-carrier mobility on the macroscopic scale.[4i,j]

Organogels[5] are excellent examples of the construction of higher order self-assembled structures from properly designed small-molecule building blocks. The formation of organogels is facilitated by the self-assembly of gelator molecules in a specific manner through various noncovalent interactions. In the recent past, several organogelators have been reported based on p-type organic semiconductors, such as porphyrins,[6] phthalocyanines,[7] oligophenylenevinylenes,[8a–d] oligophenyleneethynylenes,[8e,f] and oligothiophenes.[9] However, such examples for n-type organic semiconductors are still rare.[10]

Perylene bisimides (PBIs) have attracted extensive attention in the last few years due to their excellent n-type semiconductivity[11] and intense photoluminescence.[12] Multichromophoric assemblies based on perylene bisimide building blocks,[13] created by both covalent and noncovalent interactions, have been studied for photonic and electronic purposes. Such chromophore assemblies find various applications, for example, as light-harvesting systems,[14] photoinduced electron-transfer systems,[15] organic light-emitting diodes (OLEDs),[16] organic thin-film transistors,[17] and solar cells.[18] Various supramolecular approaches have been exploited to generate self-assembled structures based on this class of chromophores.[19] We have recently shown that PBI derivatives equipped with three long alkyl chains at the aromatic imide substituents form one-dimensional self-assembled structures in solution by π–π stacking, with dramatic concentration-dependent variations in photophysical properties.[20] To strengthen the intermolecular interaction between the functional PBI units and to increase the length of the self-assembled domain in solution, we introduced additional amide functionality at the imide substituents to facilitate hydrogen bonding in addition to the π–π stacking (**PBI-1**).[21] Indeed, the **PBI-1** molecule was found to self-assemble in a highly dilute solution and to gel a broad range of organic solvents that have varying dielectric constants. Photophysical studies in solution revealed the formation of a self-assembled structure with a hypsochromically shifted absorption band (H-aggregate). The presence of helical structures was observed in the AFM images of the gel derived from this achiral gelator.[21] It was understood that in such an organogel the PBI chromophores were stacked on top of each other with slight rotational displacement along the long axis to generate helical aggregates.[22] However, in these systems both left-handed (*M*) and right-handed (*P*) helicity was observed as expected from achiral chromophores. Thus, to explore the possibility of generating selectively one-handed helices, we synthesized another structurally similar organogelator containing chiral alkyl side chains (**PBI-3**). To our surprise, this PBI chromophore formed an aggregate with very different spectral properties, that is, a bathochromically shifted J-band, in contrast to **PBI-1**, which showed a hypsochromically shifted H-type band, and hence the gel of **PBI-3** was almost black in color.[23] Such a remarkable difference in self-assembly behavior between **PBI-1** and **PBI-3** prompted us to investigate this system in detail to gain a better insight into the role of the peripheral alkyl side chains on the self-assembly behavior. When one compares the structures of **PBI-1** and **PBI-3**, there are three obvious differences: 1) the length of the alkyl side chain is reduced from C12 (**PBI-1**) to C8 (**PBI-3**), 2) two methyl groups are introduced in **PBI-3** as branching units in each side chain, whereas all the alkyl chains are linear in **PBI-1**, 3) **PBI-3** is chiral whereas **PBI-1** is not.

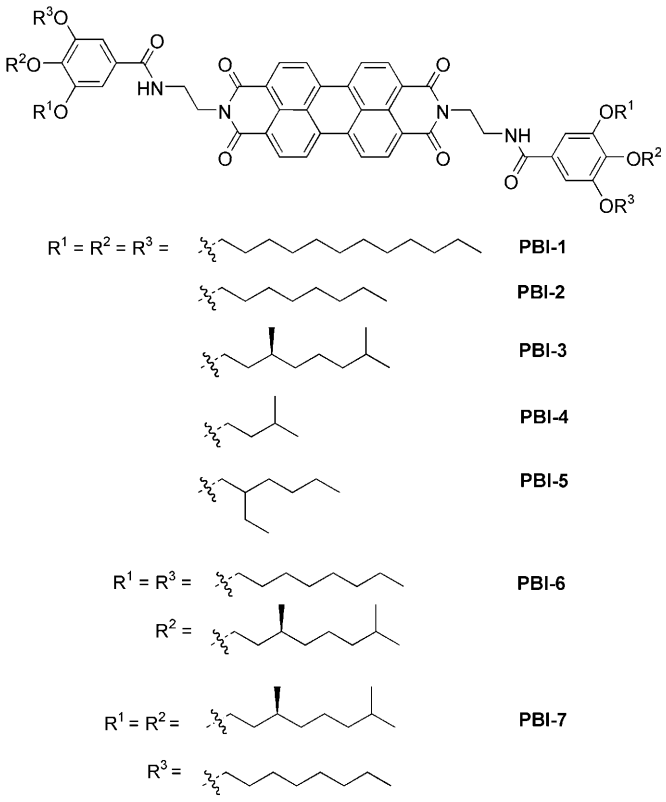

To probe individually the role of these three structural variations on self-assembly, we have synthesized a series of PBI organogelators in which the basic building block remains the same but the length as well as the nature of the alkyl substituents in the benzamide group at the imide positions are systematically varied. From **PBI-1** to **PBI-2** the length of the alkyl chain is reduced from C12 to C8, whereas in **PBI-3** all linear alkyl chains are replaced by chiral C10 chains with branching. In **PBI-6** and **PBI-7**, instead of all three, only one or two such chiral branched side chains are introduced. **PBI-4** has the similar branching units as in the case of **PBI-3** but the chirality is absent and also the chain length is much shorter. In **PBI-5** the racemic 2-ethylhexyl group has been introduced to increase the bulkiness without providing a helical bias.

Herein, we report the synthesis of this series of new PBI organogelators and give a detailed account of structure-

property relationship in terms of their self-assembly behavior and gelation capability.

Results

Synthesis: The synthetic route for various PBI organogelators is outlined in Scheme 1. Commercially available starting material 3,4,5-trihydroxymethyl benzoate was alkylated with appropriate alkyl bromides to get trialkoxymethyl benzoate **1**. For **PBI-1** to **PBI-5**, the intermediate **1** was produced in a single reaction step in about 90% yield by using 4.5 equiv of base and alkyl bromide. For **PBI-6**, 1 equiv of base and alkyl bromide was used to selectively alkylate the OH group in the 4-position of 3,4,5-trihydroxymethyl benzoate. The monoalkylated product **1′** was obtained in 61% yield. Subsequently, the remaining two OH groups were alkylated to obtain compound **1f** in 91% yield. For **PBI-7**, compound **1′** was alkylated in two successive steps; first it was reacted with the *n*-octyl bromide by controlling the molar ratio of the base as well as alkyl bromide to obtain **1″** in 40% yield and then the remaining OH group in **1″** was alkylated with the respective chiral alkyl bromide to afford **1g** in 92% yield. Once the intermediate **1** was obtained, the subsequent reaction steps were similar for all the PBI derivatives. The methyl ester was hydrolyzed by KOH base in 80–90% yield and then converted to the aminoethylbenzamide derivative **3** via the acid chloride intermediate in about 60–65% yield. All the PBI derivatives were prepared by coupling the perylene tetracarboxylic acid bisanhydride with the appropriate aminoethylbenzamide derivative **3** in the presence of $Zn(OAc)_2$ as a catalyst and were isolated as either red or black

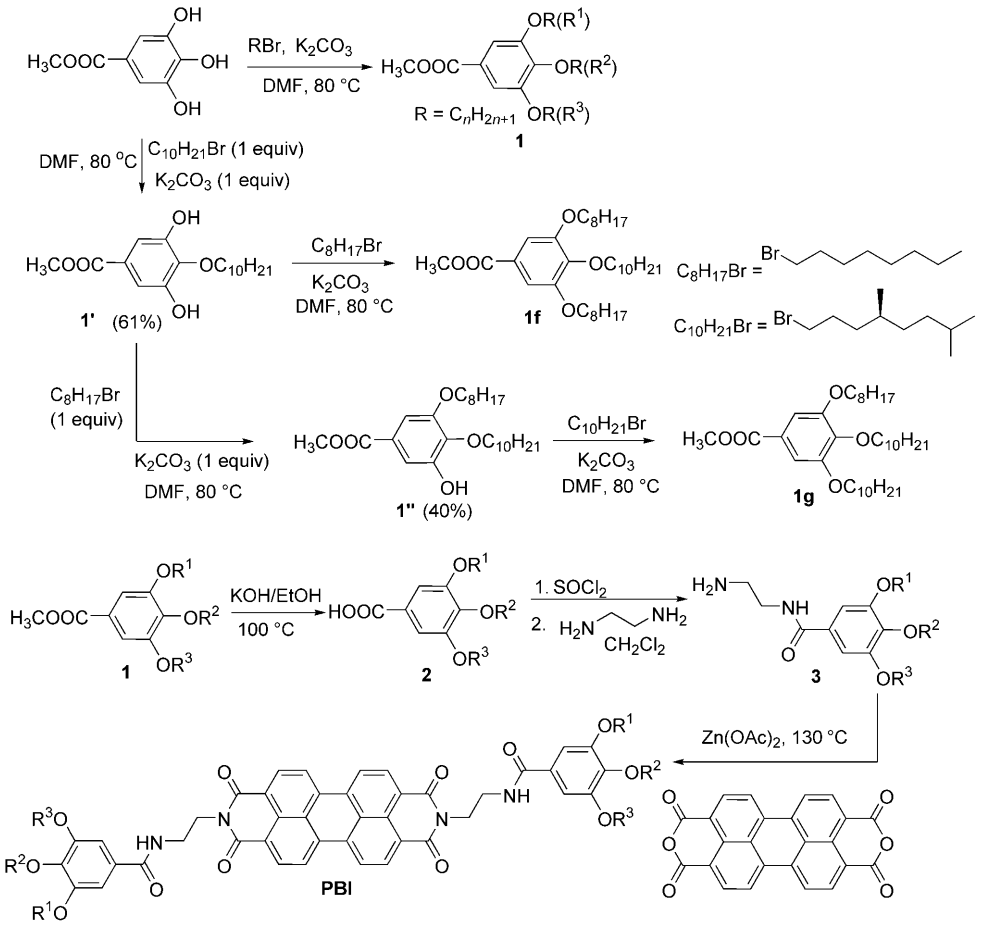

R^1=R^2=R^3=R = *n*-dodecyl: **1a** (84%), **2a** (92%), **3a** (63%), **PBI-1** (39%)
= *n*-octyl: **1b** (80%), **2b** (90%), **3b** (65%), **PBI-2** (35%)
= (*S*)-3,7-dimethyloctyl: **1c** (88%) , **2c** (91%), **3c** (61%), **PBI-3** (55%)
= 3-methylbutyl: **1d** (72%), **2d** (87%), **3d** (64%), **PBI-4** (49%)
= 2-ethylhexyl: **1e** (15%), **2e** (87%), **3e** (65%), **PBI-5** (54%)
R^1=R^3= *n*-octyl; R^2=(*S*)-3,7-dimethyloctyl: **1f** (91%), **2f** (90%), **3f** (62%), **PBI-6** (48%)
R^1=R^2=(*S*)-3,7-dimethyloctyl; R^3= *n*-octyl, **1g** (92%), **2g** (91%), **3g** (67%), **PBI-7** (50%)

Scheme 1. Synthesis of the present series of PBI derivatives.

solids in about 40–55% yield. All the final compounds as well as the intermediates were characterized by ^{1}H NMR spectroscopy, HRMS (ESI), and UV-visible spectroscopy.

Aggregation studies: The self-assembly of the present PBI derivatives was examined by solvent-dependent and variable-temperature UV-visible spectroscopy. Figure 1a shows the absorption spectra of **PBI-1** in various ratios of methyl cyclohexane (MCH) and chloroform. The latter is a good solvent for solvation of the π system of PBI dyes, hence the dyes do not form aggregates at a high $CHCl_3$ content of 50% at the concentration (1×10^{-5} M) applied in these experiments. Thus, for a 50:50 MCH/$CHCl_3$ ratio the major absorption band shows the well-resolved vibronic structure ranging from 400 to 550 nm that is characteristic for the S_0–S_1 transition of the isolated PBI chromophore. In contrast, MCH is a bad solvent for the solvation of the π system of PBI. As a consequence, the dye is not soluble in pure MCH and aggregation is observed at higher volume ratios of MCH/$CHCl_3$ as evidenced by distinct spectral changes (Figure 1a). The most prominent features are a reduction in the peak intensity along with a significant blueshift of the absorption maximum and a loss of the fine structure. Additionally, a new peak appeared at a longer wavelength of 555 nm. These features suggest the formation of face-to-face π stacks (H-aggregate) of rotationally displaced PBI chromophores.[20] For **PBI-2** and **PBI-6**, very similar H-type π stacking was observed (see the Supporting Information for details). In contrast, self-assembled π stacks of **PBI-3** and **PBI-4** exhibit a completely different optical signature. Thus, a new redshifted J-type absorption band appears at 621 nm with increasing amount of MCH and disappearance of the characteristic vibronic pattern of the monomeric dye (Figure 1b). Additionally, a hypsochromically shifted second broad band shows up at 432 nm. **PBI-7** revealed very intriguing self-assembly behavior with increasing amount of MCH; there were two new bands at 550 and 621 nm due to the formation of H- and J-type structures, respectively (Figure 1c). Analysis of the aggregate spectrum at 90:10 MCH/$CHCl_3$ revealed the presence of H- and J-aggregates approximately in a 1:1 ratio. For **PBI-5**, similar absorption spectra are measured in pure MCH and in pure $CHCl_3$ (see the Supporting Information for details), thus suggesting the absence of π stacking in dilute solution.

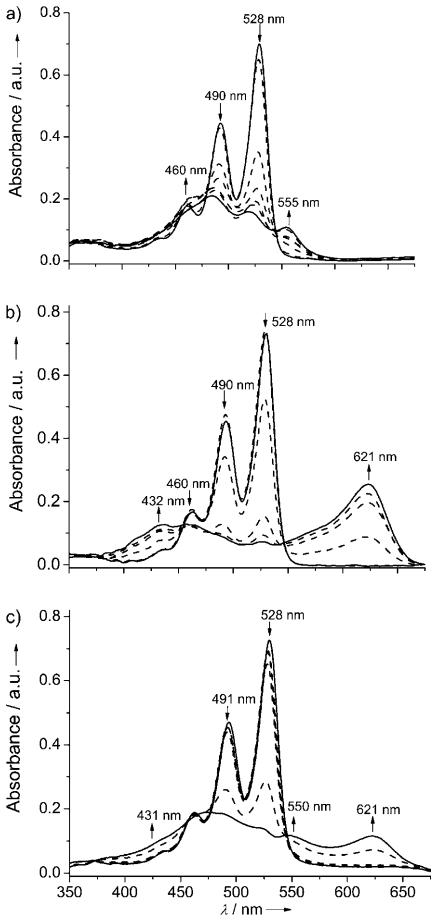

Figure 1. Solvent-dependent (in various MCH/$CHCl_3$ mixtures) UV-visible absorption spectra of a) **PBI-1** (50:50 to 80:20), b) **PBI-4** (40:60 to 70:30), and c) **PBI-7** (50:50 to 90:10) at a concentration of 1×10^{-5} M at 25°C. Arrows indicate the spectral changes upon increasing the amount of MCH (from 40 to 90%).

To quantify the propensity for π-stack formation for this series of dyes, we have estimated the mole fraction of aggregated dyes (α_{agg}) in the respective MCH/$CHCl_3$ solvent mixtures from the solvent-dependent UV-visible studies by using Equation (1).

$$\alpha_{agg} \approx \frac{A_{mix}-A_{mon}}{A_{agg}-A_{mon}} \quad (1)$$

In this equation, A_{mix} is the absorbance at 528 nm for the PBI chromophore at a given solvent mixture, whereas A_{mon} and A_{agg} denote the absorbance at 528 nm at the lowest and highest MCH/$CHCl_3$ ratios, respectively. The α_{agg} values at various solvent mixtures for all of the PBI derivatives investigated here are plotted as a function of the solvent composition in Figure 2. The critical solvent composition in which the mole fraction of the aggregate is 0.5 (α_{50}) is estimated from such a plot and the values are reported in Table 1. We

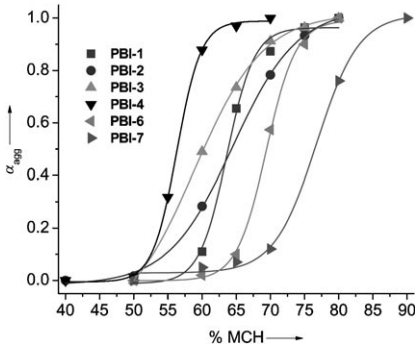

Figure 2. Plot of α_{agg} as a function of solvent composition (MCH/$CHCl_3$) for various PBI chromophores. The sigmoidal fit for the data points were obtained by using the Boltzmann function.

Table 1. The α_{50} (% of MCH in $CHCl_3$ at which the α_{agg} value is 0.5) and $\alpha_{50}(T)$ (at 80:20 MCH/$CHCl_3$) values for various PBI chromophores.

	PBI-1	PBI-2	PBI-3	PBI-4	PBI-6	PBI-7
α_{50}	64	64	60	56	69	77
$\alpha_{50}(T)$ [°C]	54	53	56	–[a]	47	31

[a] **PBI-4** was not soluble in 80:20 MCH/$CHCl_3$, thus the experiment could not be performed.

also probed the self-assembly as a function of temperature in 80:20 MCH/$CHCl_3$ solvent mixture. For this solvent composition, at 30 °C a mostly self-assembled structure was observed as expected from a previously performed solvent-dependent study. The spectral variations as a function of temperature for **PBI-6** are shown in Figure 3. With increasing

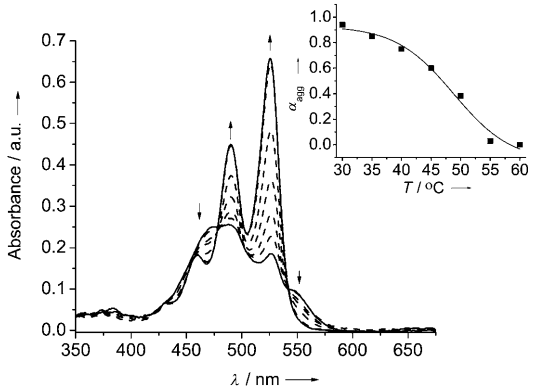

Figure 3. Temperature-dependent UV-visible absorption spectra of **PBI-6** in MCH/$CHCl_3$ mixtures (80:20) at a concentration of 1×10^{-5} M. Arrows indicate the spectral changes with an increasing temperature from 30 to 60 °C. The inset shows the mole fraction of aggregate ($\alpha_{agg}(T)$) as a function of temperature.

temperature, the band at 550 nm gradually decreases and eventually disappears at 60 °C. Further, at elevated temperature, the broad band becomes structured with pronounced peaks at 528 and 490 nm. All these observations together suggest conversion of the aggregated structure to the monomeric dye at elevated temperature. The mole fraction of aggregate at each temperature ($\alpha_{agg}(T)$) was estimated by using Equation (2):

$$\alpha_{agg}(T) \approx \frac{A(T)-A_{mon}}{A_{agg}-A_{mon}} \quad (2)$$

in which $\alpha_{agg}(T)$ is the mole fraction of aggregate at temperature T, and A_{mon}, $A(T)$, and A_{agg} are the absorbance at 528 nm for the monomer, the solution at temperature T, and the pure aggregate solutions, respectively. The $\alpha_{agg}(T)$ values were plotted as a function of temperature (see the Supporting Information for details) and from such a plot the $\alpha_{50}(T)$ (temperature at which $\alpha_{agg}=0.5$) could be estimated for various PBI derivatives (Table 1). It can be seen that these values for **PBI-1** and **PBI-2**, both of which form H-aggregate, are identical, suggesting no difference in their aggregation propensity. In contrast, for **PBI-6**, in which only one of the three achiral *n*-octyl chains of **PBI-2** is substituted by a chiral side chain, the α_{50} value increases from 64 to 69% and the $\alpha_{50}(T)$ value decreases from 53 to 47 °C. Thus, the presence of a single methyl branch at one of the alkyl side chains is already able to destabilize the H-type π-stacking mode. An even lower propensity for the formation of self-assembled π stacks is revealed by the significantly higher α_{50} and lower $\alpha_{50}(T)$ values for **PBI-7** bearing two methyl branches at each of the imide substituents. Remarkably however, for **PBI-3** bearing three methyl branches at each imide substituent, similar α_{50} and $\alpha_{50}(T)$ values are observed as for **PBI-1** and **PBI-2**. Clearly, this unexpected strengthening of π-stack stability is related to the transition to a pure J-aggregate, which suggests not much difference between the stability of the H- and J-type π stack. For **PBI-4**, the lowest α_{50} value and, accordingly, the highest π-stack stability is found among these PBI dyes, which might be attributed to an entropic effect due to the presence of much shorter (C5) alkyl substituents. It is, nevertheless, remarkable that the structurally closely related dye **PBI-5** behaves completely oppositely, that is, shows the lowest π-stack stability, which pinpoints the subtle steric effect of peripheral side chains on self-assembly.

Homo- versus heteroaggregation: As **PBI-1** and **PBI-3** form H- and J-aggregate, respectively, mixing of these two chromophores should either lead to coaggregation or self-sorting.[24] To elucidate the preferential self-assembly protocol, UV-visible spectroscopic studies were performed with the mixture of **PBI-1** and **PBI-3** in different molar ratios, while keeping the total chromophore concentration (1×10^{-5} M) constant. An 80:20 MCH/$CHCl_3$ solvent mixture was used in this study in which both **PBI-1** and **PBI-3** are known to form aggregates of their own. The UV-visible spectra of different mixtures are shown in Figure 4a. The most indicative band is the J-band at 621 nm that is formed with increasing molar ratio of **PBI-3**. Because the H-aggregate does not have any absorbance at this wavelength, this band is solely attributed to the J-aggregate. On the other hand, the J-aggregate has a significant absorbance over the whole visible wavelength range with a minimum at 550 nm. At this wavelength a maximum is given for the H-aggregates of pure **PBI-1** (compare Figure 1a). Thus, relative absorption intensities at these two wavelengths (550 and 621 nm) can be used to estimate the amount of J- and H-aggregated PBI dyes. Towards this goal the spectral contribution of the J-aggregate fraction was subtracted from the original spectrum to get the spectrum of H-aggregate fraction by using Equation (3a). Spectral contribution of only J-aggregate in each mixture was calculated by using Equation (3b).

$$S_H = S_{org} - \left(\frac{A_{621}}{A_{621}(\textbf{PBI-3})} \times S_{org}\right) \quad (3a)$$

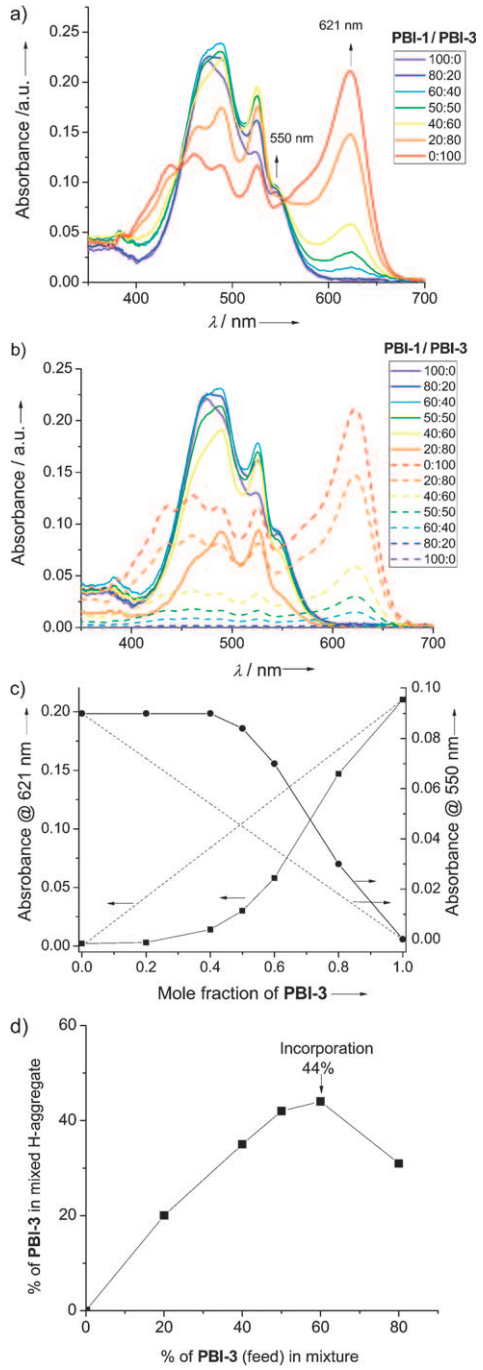

Figure 4. a) UV-visible absorption spectra of a mixture of **PBI-1** and **PBI-3** in different ratios in 80:20 MCH/$CHCl_3$ at 25 °C. The total concentration of chromophores remains constant (1×10^{-5} M) in each mixture. b) H- and J-aggregated spectral contributions S_H (——) and S_J (– – –) according to Equations (3a) and (3b), respectively. c) Change of absorbance at 550 and 621 nm in the spectra represented in b as a function of the mole fraction of **PBI-3**. Dashed lines refer to the calculated variations assuming no mixing among the two chromophores in the aggregate state. d) Plot of % **PBI-3** in the mixed H-aggregate of **PBI-1** and **PBI-3** as a function of their feed composition.

$$S_J = \frac{A_{621}}{A_{621}(\textbf{PBI-3})} \times S_{org} \qquad (3b)$$

S_H, S_J, and S_{org} correspond to the H-aggregate spectral fraction, J-aggregate spectral fraction, and the original spectrum, respectively. A_{621} and A_{621}(**PBI-3**) are the absorbance at 621 nm for a particular mixture and for pure **PBI-3**, respectively. The assumption in this calculation is that the absorption coefficient at each wavelength remains unchanged for the J-aggregate even in the mixture. The decoupled spectra for the H- and J-aggregate fractions are shown in Figure 4b and the absorbance at 550 and 621 nm for each mixture is plotted against the mole fraction of **PBI-3** in Figure 4c. Both S_H and S_J spectra in Figure 4b as well as Figure 4c clearly pinpoint a nonlinear behavior that is indicative of mixing among the two chromophores in the aggregate state. When the ratio of **PBI-1**/**PBI-3** is changed from 100:0 to 60:40, there is almost no decrease of the band intensity at 550 nm and only a very modest J-band appears at 621 nm. This suggests that **PBI-3** is incorporated into the H-aggregate of **PBI-1** up to a molar content of 40 % instead of sorting out to form its own J-aggregate. As a consequence of this coaggregation between **PBI-1** and **PBI-3** the concentration of H-aggregate remains constant for these mixtures. With further increase of the relative amount of **PBI-3**, a nonlinear increase of the absorption intensity at 621 nm is observed with a concomitant decrease of the absorption intensity at 550 nm. It is noteworthy that the absorbance at 621 nm in all mixtures is less than estimated based on the amount of **PBI-3**, whereas that for 550 nm is always enlarged. This observation suggests that **PBI-3** incorporates more easily into the H-type π stack of **PBI-1** than vice versa. If we assume that all **PBI-1** is incorporated in H-aggregates and that the absorbance at 621 nm originates from pure **PBI-3** aggregates, then the relative amount of **PBI-3** in the mixed H-aggregate (α(**PBI-3**)) in various feed compositions of the two chromophores can be estimated by using Equation (4):

$$\alpha(\textbf{PBI-3}) = \frac{[\textbf{PBI-3}]-[J]}{[\textbf{PBI-1}]+[\textbf{PBI-3}]-[J]} \times 100 \qquad (4)$$

in which [**PBI-1**] and [**PBI-3**] are the feed concentrations of the two chromophores, respectively, and [J] is the concentration of J-aggregated dyes. The extinction coefficient (ε_J) at 623 nm ($21\,000\,M^{-1}cm^{-1}$) for the aggregate spectra of pure **PBI-3** was used to calculate the [J] values in each chromophore mixture. α(**PBI-3**) values are plotted as a function of feed composition of **PBI-3** in Figure 4d. It can be seen that the maximum incorporation of **PBI-3** in the mixed stack is limited to approximately 44 %. This indicates that the ratio of **PBI-3**/**PBI-1** never exceeds 1:1 in the mixed stack.

Gelation study: Gelation ability of these PBI organogelators was tested at 1 mM concentration in toluene. At this concentration none of them were soluble in toluene at room temperature except **PBI-5**, but they could be dissolved upon heating. When the hot solution was allowed to cool down to room temperature, red gel was observed for **PBI-1**, **PBI-2**, and **PBI-6**, whereas for **PBI-3** and **PBI-4** the gel was dark

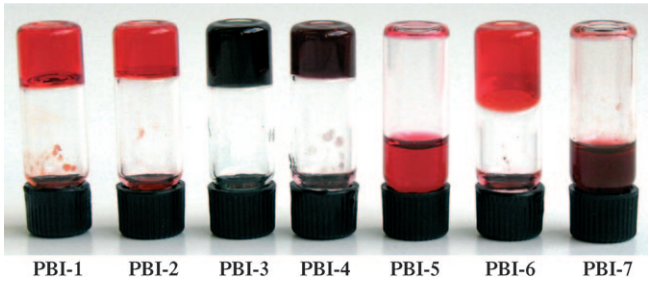

Figure 5. Pictures of gels for various PBI chromophores. In all these cases, the solution was prepared in toluene by heating the sample and the picture was taken after leaving the samples at room temperature for 30 min.

green (Figure 5). In all these cases, gelation occurred within approximately five minutes. No gelation was observed for **PBI-5** and **PBI-7**. The former was soluble in toluene, benzene, and MCH even at room temperature and remained dissolved even after a prolonged period. **PBI-7** was soluble at elevated temperature but upon cooling instead of a gel, a gel-like precipitate was formed. The critical gelation concentration (CGC) values in toluene were very low for all PBI gelators. For **PBI-1** it was 0.1–0.2 wt %, for **PBI-2** and **PBI-6** it was 0.05–0.08 wt %, and for J-aggregating **PBI-4** and **PBI-3** it was also in the range of supergelators[5e] (< 0.1 wt %).

To test the versatility of these organogelators, we further studied gelation property in different organic solvents. The results are summarized in Table 2. **PBI-1** forms a gel in a variety of solvents such as aromatic (toluene, benzene), aliphatic (MCH, hexane), ether (THF, dioxane), and triethyl amine. It does not form gel, however, in hydrogen-bond donor or hydrogen-bond acceptor solvents such as ethanol or acetone, acetonitrile, DMF, or DMSO. Gelator **PBI-2**, which has a shorter alkyl chain (C8) than **PBI-1** is effective in gelating only aliphatic and aromatic solvents. However, **PBI-3** is the most versatile gelator among the present series and was able to form a gel in every type of tested organic solvent except in DMF and DMSO. The gelation ability of **PBI-4** is quite similar to that of **PBI-3** in aromatic solvents. However, in other tested solvents it did not form a gel; either it was not soluble even at elevated temperature or precipitated out upon cooling. **PBI-6** exhibits similar gelation capabilities as structurally related **PBI-2**.

Table 2. Gelation study in various solvent systems.[a]

Solvent	PBI-1	PBI-2	PBI-3	PBI-4	PBI-6
toluene	G	G	G	G	G
benzene	G	G	G	G	G
MCH[b]	G	G	G	P	G
hexane	G	G	G	P	G
THF	G	P	G	GP	GP
dioxane	G	P	G	GP	GP
Bu_2O[c]	G	P	G	GP	GP
acetone	P	P	G	P	P
acetonitrile	P	P	G	P	P
ethanol	P	P	G	P	P
TEA[d]	G	P	G	P	GP
DMSO	P	P	P	P	P
DMF	P	P	P	P	P

[a] G, GP, and P denote gelation, gel-like precipitation, and precipitation, respectively. [b] Methylcyclohexane. [c] Dibutyl ether. [d] Triethylamine.

AFM studies: The morphology of the gels was examined by using atomic force microscopy (AFM). The AFM images of **PBI-2** in toluene are shown in Figure 6. Helical nanofibers[25] could be observed without any preferential helicity. Similar helical fibers could also be observed for the other H-aggregating PBI chromophores (see the Supporting Information for details), even though none of them possesses any chiral substituent except **PBI-6**. It is interesting to note that even for **PBI-6**, both left- and right-handed helices were present in comparable amounts (see the Supporting Information for details). Single-handed helices were observed only for chiral J-aggregating gelator **PBI-3**. For the other J-aggregating dye **PBI-4**, both handed helical fibers were observed (Figure 7) because no chiral substituent is present in this chromophore. The height and pitch of the fibers obtained for different gelators are presented in Table 3. It can be seen that the gel fibers in all these cases are almost similar in dimensions with height ranging from 2.5–4 nm whilst the pitch is quite diverse, that is, 6–15 nm. AFM morphology of **PBI-7**, which formed a mixed aggregate in solution but did not form a gel, is shown in Figure 8. In this case similar fibers are observed as well. Careful observation revealed two types of fibers, one of them shows a more ordered structure with left-handed helicity (indicated by arrow 2) with helical pitch of 11 ± 2 nm and the other (indicated by arrow 1) appears rather disordered. The height ((3.0 ± 0.2) nm) and width

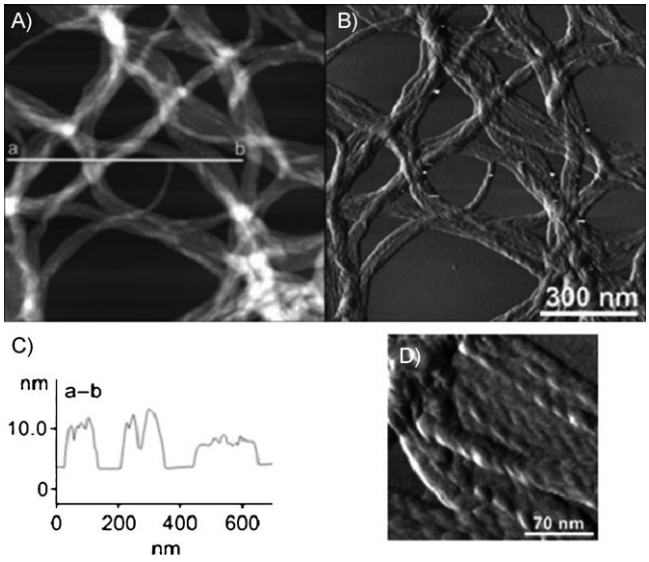

Figure 6. AFM images of **PBI-2**: A) height image, B) phase image, C) cross-section analysis, D) magnified region from image B. Diluted gel (0.3 mM) in toluene was spin-cast on mica before taking the AFM images.

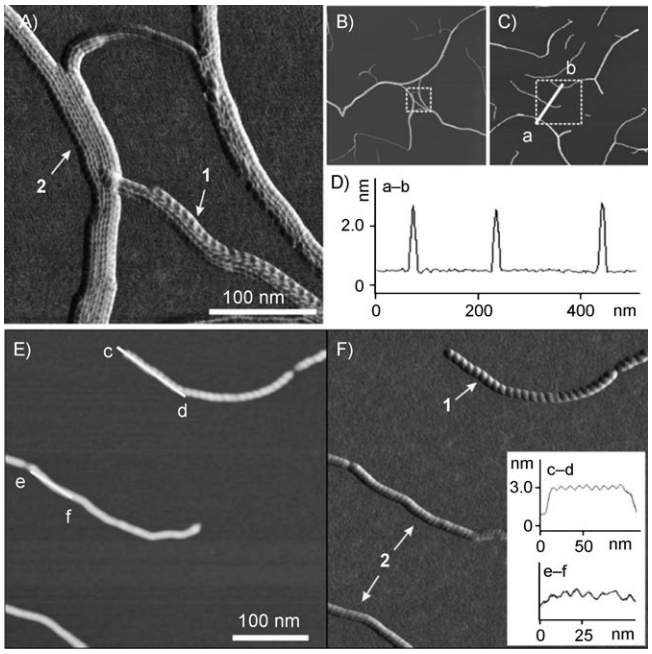

Figure 7. AFM images of **PBI-4**: A) magnified phase image from B; B, C) height images; D) cross section along line a–b in image C; E) magnified height image from C; F) phase image from E. Diluted gel (0.27 mM) in toluene was spin-cast on mica before taking the images.

Table 3. AFM data for the PBI gelators.

	PBI-1	PBI-2	PBI-3	PBI-4	PBI-6
height [nm]	3.1±0.3	3.9±0.2	2.4±0.2	2.3±0.2	3.4±0.2
pitch [nm]	15±2.0	9±0.4	6.6±0.1	11±0.2[a]	14±0.5
helicity	*P*/*M*	*P*/*M*	*P*	*P*/*M*	*P*/*M*

[a] Fibers with slightly different pitch are also observed.

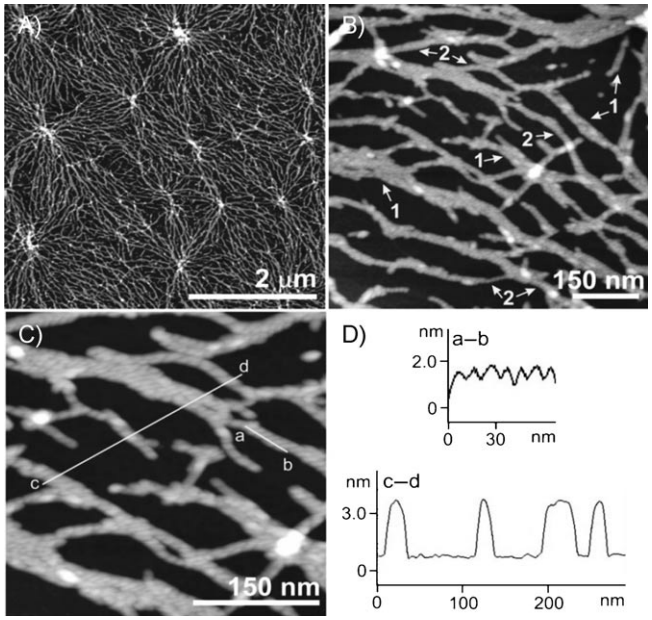

Figure 8. AFM images of **PBI-7**: A–C) height images, D) cross-sectional analysis. Diluted gel (0.3 mM) in toluene was spin-cast on mica before taking the AFM images.

((12±3) nm) of both of these structures are of similar dimensions.

Aggregation study by CD spectroscopy: As **PBI-3, PBI-6**, and **PBI-7** have chiral side chains, a helical bias is expected for their self-assembled structures.[26] Figure 9 shows the CD

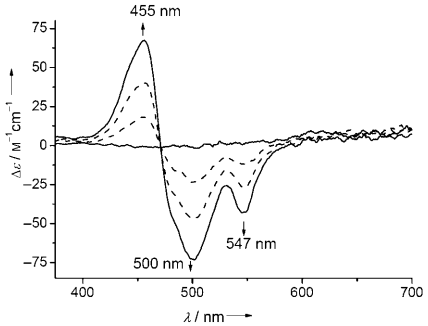

Figure 9. Solvent-dependent CD spectra of **PBI-6** in MCH/$CHCl_3$ mixtures from 55:45 to 80:20 at a concentration of 1×10^{-5} M at 25 °C. Arrows indicate the spectral changes with increasing amount of MCH.

spectra of **PBI-6** in various solvent compositions. No CD signal is observed in 55:45 MCH/$CHCl_3$ because the dye does not form any aggregate in this solvent composition. However, when the MCH content was increased above 65 % a strong bisignated Cotton effect was observed with positive and negative maxima at 455 and 500 nm, respectively. Another negative band is observed at 547 nm, which corresponds to the shoulder that arises in the UV-visible spectra upon aggregation. For **PBI-3**, the major CD signal appeared at much longer wavelength (645 nm) and accordingly relates to the J-band observed in the UV-visible spectra (Figure 1b and ref. [23]). A UV-visible spectroscopic study revealed the coexistence of H-type and J-type aggregate for **PBI-7**. Likewise, CD spectroscopic studies show spectral changes that can be attributed to two species (Figure 10). There are strong negative and positive bands at 500 and 454 nm, respectively, along with a relatively weak negative band at 545 nm. These three bands are quite similar to those ob-

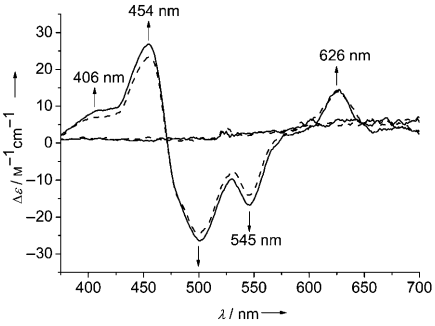

Figure 10. Solvent-dependent CD spectra of **PBI-7** in MCH/$CHCl_3$ mixtures from 55:45 to 90:10 at a concentration of 1×10^{-5} M in a 1 cm cuvette at 25 °C. Arrows indicate the spectral changes with increasing amount of MCH.

served in the case of **PBI-6** and thus can be attributed to H-aggregated species. However, two more bands are seen at 626 and 406 nm that resemble those found for **PBI-3** (see the Supporting Information for details) and are thus evidence for the presence of J-aggregated species. Furthermore, temperature-dependent CD spectroscopy experiments for **PBI-6** solutions confirmed the reversibility of the self-assembly process (see the Supporting Information for details). At 25 °C in a 80:20 MCH/$CHCl_3$ mixture, there was a strong excitonic CD couplet, indicating the presence of chiral aggregate. When the temperature was raised, the intensity of the CD signal decreased and almost disappeared at 60 °C, which revealed conversion of the aggregate structures into monomers.

Coaggregation of **PBI-1** and **PBI-3** was also studied by using CD spectroscopy (Figure 11). The experiments were done under identical conditions as the UV-visible spectroscopy experiments. It can be seen that with 100% **PBI-1**, there is no CD signal (violet line) because the H-aggregating chromophore **PBI-1** does not possesses any chiral side chain. However, when 20% of J-aggregating chromophore **PBI-3** was added to 80% of **PBI-1**, a strong excitonic-type CD band appeared (blue line) with a positive and negative maximum at 458 and 499 nm, respectively, along with a second negative band at 546 nm. With further increase in the amount of **PBI-3** up to 60% in the mixture, there was little change in the band intensities at 458, 498, and 546 nm[27] but a separate band appeared at 623 nm due to the formation of pure J-aggregate by **PBI-3** (orange line). At 20:80 **PBI-1**/**PBI-3** a significant decrease of the intensity of the excitonic CD signal is observed that can be rationalized in terms of the lowered concentration of H-aggregate (pink line). Notably, these results corroborate well to the UV-visible results shown in Figure 4.

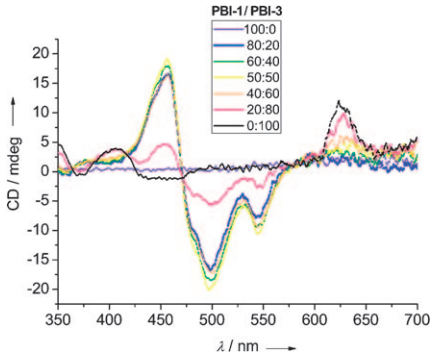

Figure 11. CD spectra of **PBI-1** and **PBI-3** in different ratios in MCH/$CHCl_3$ mixtures (80:20) at 25 °C. Total concentration of the chromophores were kept constant (1×10^{-5} M) in each mixture.

We also examined the possibility of a preferential population of one-handed helices by external chiral bias imparted by a suitable chiral solvent.[28] The chiral solvent limonene has been used in this study due to its structural similarity with toluene, in which the self-assembly of **PBI-1** chromophore had been studied before.[21] Variable-temperature UV-visible spectroscopic studies of **PBI-1** in (*R*)- and (*S*)-limonene confirmed the formation of H-aggregate at ambient temperature (see the Supporting Information for details). In Figure 12, temperature-dependent CD spectra of **PBI-1** in (*R*)-limonene are shown. At elevated temperature, no Cotton effect was observed, suggesting the absence of any aggregated structure. However, when the solution was cooled, a strong Cotton effect was observed with positive and negative maxima at 458 and 499 nm, respectively, along with another negative band at 546 nm. The shape of the CD spectrum is identical to that for chiral chromophore **PBI-6** in the presence of excess MCH in $CHCl_3$ (Figure 9). It is also noteworthy that the $\Delta\varepsilon$ values in Figures 9 and 12 are similar in magnitude, which suggests a comparable helical bias imparted by the chiral side chain in **PBI-6** and the chiral solvent for **PBI-1**.[29] When similar variable-temperature studies were carried out in (*S*)-limonene, the CD spectra observed were exact mirror images of those found in the case of (*R*)-limonene (Figure 12).

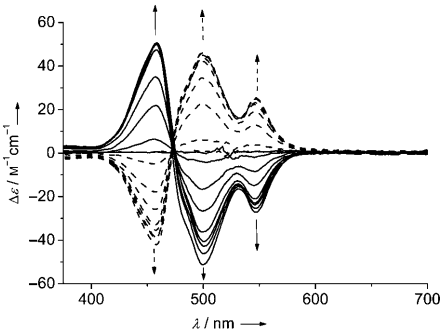

Figure 12. Temperature-dependent CD spectra of **PBI-1** in (*S*)-limonene (-----) and (*R*)-limonene (——); concentration: 5×10^{-5} M. Arrows indicate the spectral changes with decreasing temperature (100 to 30 °C).

Stirring effect: In the recent past, there has been significant interest in macroscopic orientation of supramolecular nanofibers by external perturbation such as stirring, shaking, and so forth.[30] Stirring is particularly interesting because its direction as well as the speed can be controlled precisely. Aida and co-workers have reported remarkable vortex effects on the CD signal of zinc porphyrin nanofibers,[30a] which were attributed to the alignment of the nanofibers macroscopically in the direction of the vortex flow. At the same time, Meijer and co-workers reported similar behavior of supramolecular nanostructures generated from oligo(*p*-phenylenevinylene) derivatives.[30b] To the best of our knowledge, no such studies have been reported for organogelators or for perylene bisimide dye aggregates so far. Thus, we have studied the impact of vortex flow created by a magnetic stirring bar on the CD spectra of H-aggregated achiral chromophore **PBI-1** in toluene. In the absence of stirring no CD signal was observed. However, upon clockwise stirring a very strong bisignated CD signal with a positive band at

458 nm and two negative bands at 498 and 546 nm were observed (Figure 13a). With gradual increase of the stirring speed, the CD signal intensity increased steadily before it

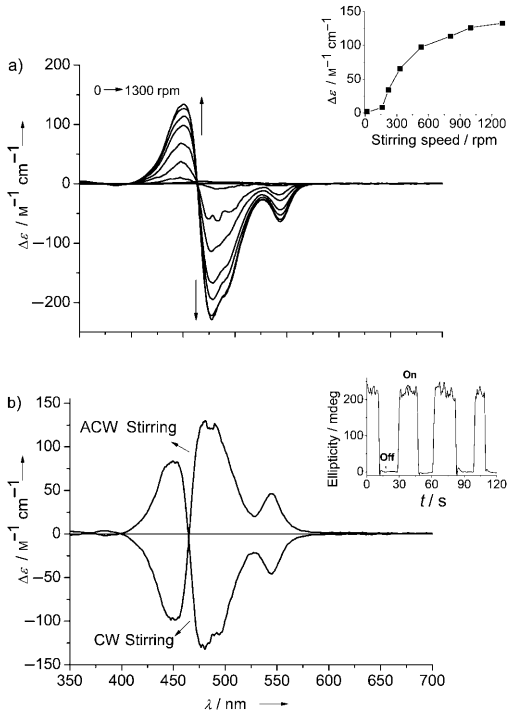

Figure 13. a) Evolution of CD signal upon gradual increase in stirring (clockwise direction) speed for a solution of **PBI-1** (5×10^{-5} M) in toluene at 30 °C; inset shows the variation of CD intensity at 446 nm as a function of stirring speed. b) Evolution of CD signal upon stirring (1300 rpm) in clockwise (CW) and anticlockwise (ACW) direction for a solution of **PBI-1** (5×10^{-5} M) in toluene at 30 °C; the inset shows the CD intensity at 446 nm with successive on–off cycles of stirring at 1300 rpm.

was saturated at about 1000 rpm (inset, Figure 13a). If the CD signal arises in this case from the vortex-induced macroscopic orientation of the supramolecular fibers, the direction of it should be altered when the stirring direction is reversed. Indeed, such dynamic behavior is observed upon changing from clockwise to anticlockwise stirring where a mirror-image CD spectrum originates (Figure 13b). Further evidence for the dynamic nature of the macroscopic aggregate orientation is given by the instantaneous on–off switching of the CD signal upon switching the magnetic stirrer on and off (inset, Figure 13b). When the stirrer was on, a strong CD signal could be observed but as soon as it was switched off, the CD signal intensity decreased to zero. This experiment was repeated for several cycles and identical results were obtained, which suggests the complete reversibility of the macroscopic orientation of the PBI aggregates by external stirring. A linear dichroism (LD) signal was also observed under vortex flow that does not alter the sign upon reversal of the stirring direction (see the Supporting Information, Figure S12). The remarkable similarity of our results with those recently published in the literature for two other dye aggregates[30] corroborates the orientation of self-assembled nanofibers by vortex flow, which might be a particularly appealing technique for the orientation of functional materials based on organogelators.

Discussion

Spectroscopic studies revealed distinct differences among the present PBI derivatives in terms of their self-assembly and gelation properties depending on the peripheral alkyl substituents. It was found that **PBI-1**, **PBI-2**, and **PBI-6** form H-aggregates, whereas **PBI-3** and **PBI-4** form J-aggregates, and **PBI-7** forms mixtures of H- and J-aggregates. On the other hand, **PBI-5** does not form any aggregate at all in the investigated concentration range. In our previous work on **PBI-1** and **PBI-3**, we proposed that the transition from H- to J-type aggregate may originate from a simple rotation around the CH_2–N_{amide} bond[23] with retention of the synergetic effect of π–π stacking and hydrogen-bonding interaction among the amide functionality as shown on the right side of Figure 14. However, it was not clear how such very subtle modification in the alkyl side chains could dictate the preference for one of these two possible π-stacking modes. Comparison of the self-assembly of **PBI-3** and **PBI-4** eliminates any specific role of alkyl chain length or chirality, because the former chromophore is substituted with chiral C10 alkyl groups, whereas the latter is with achiral C5 alkyl groups, but both of them form J-aggregate. Based on the results obtained in the present study, we propose that the bulkiness of the methyl groups in the γ position of the peripheral side chains destabilizes the more densely packed face-to-face H-type π stacking and favors the J-type π stacking, in which the chromophores are packed with significant longitudinal displacement (arrow in Figure 14, right-hand side). Owing to this displacement an increased columnar cross section is available that provides more space to accommodate the alkyl side chains. Thus, **PBI-1** and **PBI-2** having linear alkyl substituents prefer to self-assemble as more compact H-aggregates as does **PBI-6** having only one branched chain among the three alkyl substituents at each imide position, whereas **PBI-3** and **PBI-4**, both of which contain three branched alkyl substituents, prefer to self-assemble as J-aggregates in which the chromophores are packed with relatively larger space as shown in Figure 14 (middle). **PBI-7** has one linear and two branched alkyl substituents and in this case neither of the two types of stacking is largely favored. Therefore, in this case neither H-type nor J-type aggregate is formed with high preference. Notably, for this compound aggregation required the highest amount of MCH in the MCH/$CHCl_3$ mixture and the lowest temperature (Table 1), while no gelation of any tested organic solvents could be observed. This remarkably different behavior of **PBI-7**, compared with the very similar compounds **PBI-6** and **PBI-3**, can now be traced back to the disorder in packing imparted by the coexistence of H- and J-type packing modes in small domains that do not grow into well-ordered extended macroscopic fibers (Figure 8). For **PBI-5**, the pres-

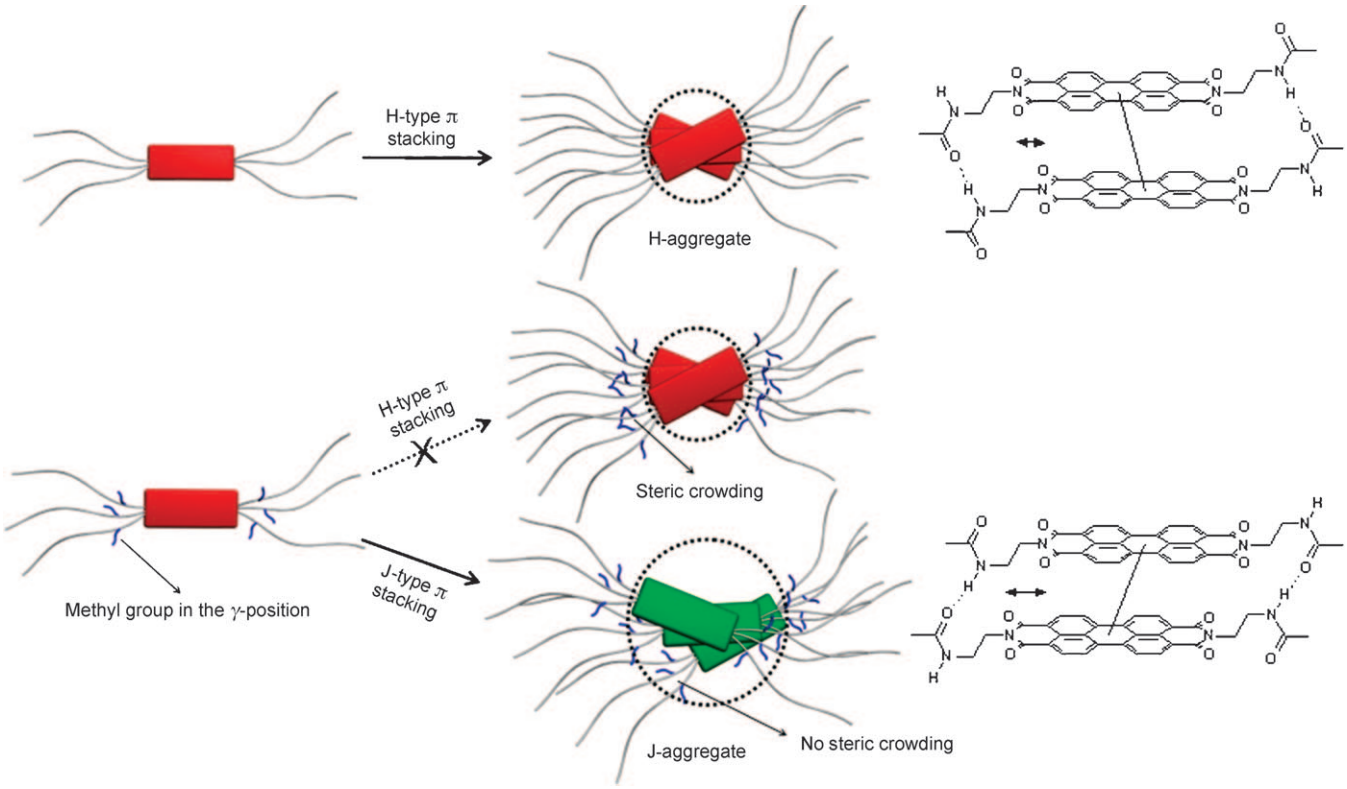

Figure 14. Left: Schematic representation of PBI chromophores with linear (top) and branched (bottom) alkyl substituents. Middle: The transition from H- (top) to J-type (bottom) π stacking with increasing steric demand of the peripheral alkyl side chains. Right: Packing model for H- (top) and J-type (bottom) π stacking. In both cases additional rotational offsets are needed to enable both close π–π contact and hydrogen bonding.

ence of larger ethyl groups at the more central β position inhibits formation of any π stacking.

Further indirect support for this hypothesis based on steric constraint is gathered from the coaggregation studies of **PBI-1** and **PBI-3**. It was found from UV-visible spectroscopy as well as from CD spectroscopic studies that, when purely J-aggregating chromophore **PBI-3** was mixed with purely H-aggregating **PBI-1**, at lower **PBI-3**/**PBI-1** ratio, only H-aggregate was formed containing both kinds of chromophores. The maximum incorporation of **PBI-3** in such a mixed H-type π stack was calculated to be 44%. This ratio implies that **PBI-3** is incorporated in the mixed H-type stack until it can be located in-between two **PBI-1** units (at the most 50% **PBI-3** can be incorporated in the mixed stack to make this arrangement possible), so that the unfavorable steric constraint among two adjacent face-to-face stacked **PBI-3** units does not arise. The ratio of 1:1 would imply a perfectly alternating arrangement of the two different chromophores in the mixed H-type stack, which is, however, not entropically favored. At a ratio of 0.44:0.56, there is still some disorder in the mixed-stacked system leading to the lowest Gibbs energy. In contrast, self-sorting of **PBI-1** and **PBI-3** dyes prevails at high **PBI-3** content due to the energetically disfavored packing of **PBI-1** dyes in a J-type packing mode.

Conclusion

We have investigated the influence of peripheral alkyl side chains on the self-assembly and gelation properties of a series of structurally related PBI chromophores. It was found that, depending on the nature of the alkyl substituents, the π-stacking mode of the chromophores could be altered from commonly seen H type to the rather uncommon J type.[31,32] Our studies revealed that steric effects in the peripheral side chains dictate the mode of self-assembly. PBI chromophores substituted with linear alkyl chain (least steric demand) formed sandwich-type H-aggregates whereas PBI chromophores bearing branched alkyl groups (higher steric demand) formed slipped J-aggregates,[32] or no aggregates at all. For mixtures of H- and J-aggregating chromophores **PBI-1** and **PBI-3** coaggregation in H-type π stacks was observed in the presence of larger amounts of the H-aggregating chromophore **PBI-1** up to a 1:1 ratio. Whilst such coaggregation suggests the intimate alternate packing of the two chromophores at a 1:1 ratio, self-sorting of **PBI-1** and **PBI-3** dyes prevails at high **PBI-3** content due to the energetically disfavored packing of **PBI-1** within J-aggregates. The results of this work may be important for the emerging field of systems chemistry.[24,33] They offer the relevant guidelines for a rational design of PBI J-aggregates. Having understood the self-assembly properties at the supramolec-

ular level, we are currently engaged in exploiting these materials in bulk heterojunction solar cells.[34]

Experimental Section

Materials and methods: All solvents and reagents were purchased from commercial sources and purified by using standard methods.[35] The solvents for spectroscopic studies were of spectroscopic grade and used as received. ^{1}H NMR spectra were recorded on a 400 MHz Bruker spectrometer and all the spectra were calibrated against tetramethylsilane (TMS). UV-visible spectra were measured by using a Perkin-Elmer Lambda 40P spectrometer equipped with a Peltier system as temperature controller. The CD spectra were recorded with a Jasco J-810 spectropolarimeter. AFM measurements were carried out under ambient conditions by using a MultiMode Nanoscope IV system operating in tapping mode in air. Silicon cantilevers (OMCL-AC160TS) with a resonance frequency of ≈300 kHz were used.

UV-visible and CD spectroscopic studies: Stock solutions (concentration 1×10^{-4} M) of PBI dyes were made in $CHCl_3$. A 0.2 mL aliquot of the stock solution was transferred to six different volumetric flasks, each of 2 mL volume. The final volume was adjusted by adding different amounts of $CHCl_3$ and methyl cyclohexane (MCH) in different flasks to get various solutions of the same concentration (1×10^{-5} M) but in different solvent compositions. The solutions were allowed to equilibrate for 3 h prior to the spectroscopic measurements. For the coaggregation studies, stock solutions of **PBI-1** and **PBI-3** in $CHCl_3$ were mixed in various ratios and then MCH was added. For variable-temperature UV-visible and CD spectroscopic experiments, a 20 min interval was given before each measurement after the desired temperature was reached.

Gelation tests: The measured amount of PBI gelator and appropriate solvent were put together in a screw-capped sample vial and it was heated until all the solute was dissolved and then allowed to cool down to room temperature. After leaving the sample for 1 h at ambient temperature, the formation of gel was tested by the "stable-to-inversion of a vial" method.[5d]

AFM studies: For AFM studies, the gel in toluene was diluted and then was spin-coated onto mica under 2000 rpm rotating speed.

Synthesis and characterization: Synthesis and characterization of **PBI-1**[21] and **PBI-3**[23] were described previously. All the other PBI organogelators investigated here were synthesized by means of a similar procedure.

4-[(*S*)-3,7-Dimethyloctyloxy]-3,5-dihydroxymethyl benzoate (1′): A mixture of 3,4,5-trihydroxymethyl benzoate (3.23 g, 17.50 mmol), (*S*)-3,7-dimethyloctyl bromide (3.62 g, 17.50 mmol), and K_2CO_3 (2.42 g, 17.50 mmol) in dry DMF (30 mL) was stirred at 80 °C for 24 h under an inert atmosphere. The reaction mixture was cooled to room temperature and poured into ice-cold water (200 mL) and was extracted with diethyl ether (3×50 mL). The combined organic layer was dried over Na_2SO_4 and the solvent was evaporated to get the crude product as a brown oil, which was purified by using column chromatography (silica gel, chloroform) to get the pure product as a light brown oil (61 %). ^{1}H NMR (400 MHz, $CDCl_3$, TMS, 300 K): $\delta=7.20$ (s, 2H), 5.52 (s, 2H), 4.16–4.12 (m, 2H), 3.87 (s, 3H), 1.86–1.13 (m, 10H), 0.94–0.85 ppm (m, 9H); UV/Vis (CH_2Cl_2): λ_{max} (ε) = 306 (1300), 295 (1800), 260 nm (7900 $M^{-1}cm^{-1}$); HRMS (ESI): *m*/*z* calcd for $C_{18}H_{27}O_5$ $[M-H]^-$: 323.1864; found: 323.1864.

3-Octyloxy-4-[(*S*)-3,7-dimethyloctyloxy]5-hydroxymethyl benzoate (1′): Compound **1′** (1.56 g, 4.81 mmol), *n*-octyl bromide (0.929 g, 4.81 mmol), and K_2CO_3 (0.663 g, 4.81 mmol) were taken in a flask along with dry DMF (20 mL) and the reaction mixture was stirred at 80 °C for 24 h under an inert atmosphere. The heating was stopped, the reaction mixture was cooled to room temperature, then poured into ice-cold water (120 mL), and extracted with diethyl ether (3×30 mL). The combined organic layer was dried over Na_2SO_4 and the solvent was evaporated to get the crude product as a brown oil. It was purified by using column chromatography (silica gel, chloroform) to get the pure product as a light yellow oil (40 %). ^{1}H NMR (400 MHz, $CDCl_3$, TMS, 300 K): $\delta=7.28$ (s, 1H), 7.16 (s, 1H), 5.82 (s, 1H), 4.20 (t, 2H), 4.01 (m, 6H), 3.87 (s, 3H), 1.84–1.14 (m, 22H), 0.93–0.85 ppm (m, 21H); UV/Vis (CH_2Cl_2): λ_{max} (ε) = 305 (2100), 268 nm (9200 $M^{-1}cm^{-1}$); HRMS (ESI): *m*/*z* calcd for $C_{26}H_{45}O_5$ $[M+H]^+$: 437.3261; found: 437.3269.

3,4,5-Tris(octyloxy)methyl benzoate (1b): 3,4,5-Trihydroxymethyl benzoate (5.0 g, 0.027 mol) was dissolved in dry DMF (50 mL) and to this solution K_2CO_3 (16.76 g, 0.121 mol) and *n*-octyl bromide (17.19 g, 0.089 mol) were added, and the reaction mixture was stirred at 70 °C for 48 h, then cooled to room temperature and poured into ice-cold water (300 mL). A light brown oil was separated from the mixture and was then extracted with diethyl ether (3×50 mL), and the combined organic layer was washed with water and brine and dried over Na_2SO_4. The solvent was evaporated and the crude product (80 %) was found to be adequately pure from TLC analyses and ^{1}H NMR spectroscopy. Thus, the product was used for the next step as such. ^{1}H NMR (400 MHz, $CDCl_3$, TMS, 300 K): $\delta=6.93$ (s, 2H), 3.96–3.92 (m, 6H), 3.88 (s, 3H), 1.71 (m, 6H), 1.33–1.25 (m, 30H), 0.96 ppm (m, 9H); UV/Vis (CH_2Cl_2): λ_{max} (ε) = 301 (4520), 274 nm (9200 $M^{-1}cm^{-1}$); HRMS (ESI): *m*/*z* calcd for $C_{32}H_{56}NaO_5$ $[M+Na]^+$: 543.4020; found: 543.4020.

Compounds **1d–1g** were synthesized according to the above-described procedure for compound **1b**.

3,4,5-(Tris-3-methylbutyloxy)methyl benzoate (1d): Light green oil (72 %); ^{1}H NMR (400 MHz, $CDCl_3$, TMS, 300 K): $\delta=7.26$ (s, along with residual solvent peak), 4.05–4.01 (m, 6H), 3.89 (s, 3H), 0.97–0.93 ppm (m, 18H); UV/Vis (CH_2Cl_2): λ_{max} (ε) = 301 (4590), 274 nm (9660 $M^{-1}cm^{-1}$); HRMS (ESI): *m*/*z* calcd for $C_{23}H_{38}NaO_5$ $[M+Na]^+$: 417.2611; found: 417.2586.

3,4,5-(Tris-2-ethylhexyloxy)methyl benzoate (1e): Light green oil (15 %); ^{1}H NMR (400 MHz, $CDCl_3$, TMS, 300 K): $\delta=7.24$ (s, 2H), 3.90–3.81 (m, 11H), 1.54–0.88 ppm (m, 43H); UV/Vis (CH_2Cl_2): λ_{max} (ε) = 301 (4470), 274 nm (9180 $M^{-1}cm^{-1}$); HRMS (ESI): *m*/*z* calcd for $C_{32}H_{57}O_5$ $[M+H]^+$: 521.4200; found: 521.4201.

4-[(*S*)-3,7-Dimethyloctyloxy]-3,5-dioctyloxymethyl benzoate (1f): Yield: 91 %; ^{1}H NMR (400 MHz, $CDCl_3$, TMS, 300 K): $\delta=7.24$ (s, 2H), 4.00–3.98 (m, 6H), 3.88 (s, 3H) 1.82–0.85 ppm (m, 49H); UV/Vis (CH_2Cl_2): λ_{max} (ε) = 301 (4620), 274 nm (9350 $M^{-1}cm^{-1}$); HRMS (ESI): *m*/*z* calcd for $C_{34}H_{61}O_5$ $[M+H]^+$: 549.4513; found: 549.4522.

3,4-[Bis-(*S*)-3,7-dimethyloctyloxy]-5-(octyloxy)methyl benzoate (1g): Light yellow oil (92 %); ^{1}H NMR (400 MHz, $CDCl_3$, TMS, 300 K): $\delta=$ 7.26 (s, 2H), 4.05–4.00 (m, 6H), 3.99 (s, 3H), 1.84–1.13 (m, 32H), 0.94–0.85 ppm (m, 21H); UV/Vis (CH_2Cl_2): λ_{max} (ε) = 301 (4600), 274 nm (9310 $M^{-1}cm^{-1}$); HRMS (ESI): *m*/*z* calcd for $C_{36}H_{65}O_5$ $[M+H]^+$: 577.4826; found: 577.4818.

3,4,5-Tris(octyloxy)benzoic acid (2b): KOH (5.6 g) was dissolved in water (40 mL) and was added to a solution of **1b** in ethanol (9.0 g, 40 mL), and the emulsion was stirred at 100 °C for 5 h. After 1 h, the emulsion became a clear solution, indicating the progress of the reaction. After 5 h, the heating was stopped and the reaction mixture was poured into a solution of concentrated HCl (15 mL) in ice-cold water (350 mL). A white precipitate came out, which was filtered and washed with distilled water and dried under vacuum. The crude product was obtained as a white powder (90 %), which was taken to the next step without further purification. M.p. 66–68 °C; ^{1}H NMR (400 MHz, $CDCl_3$, TMS, 300 K): $\delta=10.6$ (broad peak, 1H), 7.03 (s, 2H), 3.99–3.93 (m, 6H), 1.72 (m, 6H), 1.33–1.25 (m, 30H), 0.96 ppm (t, $J=7.08$ Hz, 9H); UV/Vis (CH_2Cl_2): λ_{max} (ε) = 303 (4470), 276 nm (8470 $M^{-1}cm^{-1}$); HRMS (ESI): *m*/*z* calcd for $C_{31}H_{54}NaO_5$ $[M+Na]^+$: 529.3863; found: 529.3863.

Compounds **2d–2g** were synthesized according to the above-described procedure for compound **2b**.

3,4,5-(Tris-3-methylbutyloxy)benzoic acid (2d): White powder (87 %); m.p. 75 °C; ^{1}H NMR (400 MHz, $CDCl_3$, TMS, 300 K): $\delta=7.33$ (s, 2H), 4.06 (m, 6H), 1.89–1.61 (m, 9H). 0.97–0.96 ppm (m, 18H); UV/Vis (CH_2Cl_2): λ_{max} (ε) = 303 (5100), 276 nm (9700 $M^{-1}cm^{-1}$); HRMS (ESI): *m*/*z* calcd for $C_{22}H_{36}NaO_5$ $[M+Na]^+$: 403.2455; found: 403.2455.

3,4,5-(Tris-2-ethylhexyloxy)benzoic acid (2e): Light yellow waxy material (87%); ^{1}H NMR (400 MHz, $CDCl_3$, TMS, 300 K): $\delta = 7.25$ (s, 2H), 3.81 (m, 6H), 1.67–0.86 ppm (m, 43H); UV/Vis (CH_2Cl_2): λ_{max} (ε) = 303 (5100), 276 nm (9700 $M^{-1}cm^{-1}$); HRMS (ESI): *m/z* calcd for $C_{31}H_{53}O_5$ $[M-H]^-$: 505.3898; found: 505.3899.

4-[(*S*)-3,7-Dimethyloctyloxy]-3,5-di(octyloxy)benzoic acid (2f): White waxy material (90%); ^{1}H NMR (400 MHz, $CDCl_3$, TMS, 300 K): $\delta = 7.19$ (s, 2H), 4.00–3.97–3.88 (m, 6H), 1.82–0.85 ppm (m, 49H); UV/Vis (CH_2Cl_2): λ_{max} (ε) = 303 (4900), 276 nm (8700 $M^{-1}cm^{-1}$); HRMS (ESI): *m/z* calcd for $C_{33}H_{57}O_5$ $[M-H]^-$: 533.4211; found: 533.4215.

3,4-[Bis-(*S*)-3,7-dimethyloctyloxy]-5-octyloxybenzoic acid (2g): White powder (91%); m.p. 60–62°C; ^{1}H NMR (400 MHz, $CDCl_3$, TMS, 300 K): $\delta = 7.31$ (s, 2H), 4.09–4.00 (m, 6H), 1.85–1.14 (m, 32H), 0.95–0.85 ppm (m, 21H); UV/Vis (CH_2Cl_2): λ_{max} (ε) = 303 (4900), 276 nm (8700 $M^{-1}cm^{-1}$); HRMS (ESI): *m/z* calcd for $C_{35}H_{61}O_5$ $[M-H]^-$: 561.4525; found: 561.4527.

3,4,5-Tris(octyloxy)benzoylaminoethylamide (3b): Compound **2b** (2.88 g, 5.69 mmol) was dissolved in dry dichloromethane (30 mL). Thionyl chloride (15 mL) was added along with 3 drops of dry DMF. The reaction mixture was stirred at room temperature for 12 h. The stirring was stopped and the solvents were evaporated under vacuum. The crude product was obtained as a light yellow solid and it was taken to the next step without further purification. It was redissolved in dry dichloromethane (30 mL) and the solution was added dropwise to an ice-cold flask containing ethylene diamine (30 mL). The reaction mixture was stirred in the same ice bath for another 3–4 h and then at room temperature for 12 h. Then the reaction mixture was diluted with dichloromethane (60 mL) and washed with water, aqueous $NaHCO_3$, and brine. The organic layer was dried over Na_2SO_4 and the solvent was evaporated to get the crude product, which was then added to ethanol (60 mL) and kept in the refrigerator for 2 h. The precipitate was filtered under vacuum and dried to get the crude product as a light yellow waxy material (65%). It was taken to the next step without further purification. ^{1}H NMR (400 MHz, $CDCl_3$, TMS, 300 K): $\delta = 8.00$ (broad peak, 1H), 6.91 (s, 2H), 3.94 (m, 6H), 3.46 (m, 2H), 2.95 (m, 2H), 1.71 (m, 6H), 1.33–1.25 (m, 30H), 0.96 ppm (t, 9H); UV/Vis (CH_2Cl_2): λ_{max} (ε) = 295 (3120), 264 nm (9540 $M^{-1}cm^{-1}$); HRMS (ESI): *m/z* calcd for $C_{33}H_{61}N_2O_4$ $[M+H]^+$: 549.4625; found: 549.4626.

Compounds **3d–3g** were synthesized according to the above-described procedure for compound **3b**.

3,4,5-(Tris-3-methylbutyloxy)benzoylaminoethylamide (3d): Light yellow solid (64%); m.p. 96°C; ^{1}H NMR (400 MHz, $CDCl_3$, TMS, 300 K): $\delta =$ 6.98 (s, 2H), 6.59 (broad peak, 1H), 4.05–3.98 (m, 6H), 3.48 (m, 2H), 2.93 (m, 2H), 1.71–1.61 (m, 9H), 0.96–0.94 ppm (m, 18H); UV/Vis (CH_2Cl_2): λ_{max} (ε) = 295 (3110), 264 nm (9530 $M^{-1}cm^{-1}$); HRMS (ESI): *m/z* calcd for $C_{24}H_{43}N_2O_4$ $[M+H]^+$: 423.3217; found: 423.3217.

3,4,5-(Tris-2-ethylhexyloxy)benzoylaminoethylamide (3e): Light yellow waxy material (65%); ^{1}H NMR (400 MHz, $CDCl_3$, TMS, 300 K): $\delta = 6.97$ (s, 2H), 6.55 (broad, 1H), 4.02–3.99 (m, 6H), 3.51–3.40 (m, 2H), 2.94 (m, 2H), 1.54–1.30 (m, 27H), 0.91–0.88 ppm (m, 18H); UV/Vis (CH_2Cl_2): λ_{max} (ε) = 295 (3150), 264 nm (9530 $M^{-1}cm^{-1}$); HRMS (ESI): *m/z* calcd for $C_{33}H_{61}N_2O_4$ $[M+H]^+$: 549.4625; found 549.4625.

4-[(*S*)-3,7-Dimethyloctyloxy]-3,5-di(octyloxy)benzoylaminoethylamide (3f): Light yellow waxy material (62%); ^{1}H NMR (400 MHz, $CDCl_3$, TMS, 300 K): $\delta = 6.98$ (s, 2H), 6.54 (broad, 1H), 4.02–3.99 (m, 6H), 3.50–3.46 (m, 2H), 2.95 (t, 2H), 1.82–0.85 ppm (m, 49H); UV/Vis (CH_2Cl_2): λ_{max} (ε) = 295 (3330), 264 nm (9670 $M^{-1}cm^{-1}$); HRMS (ESI): *m/z* calcd for $C_{35}H_{64}N_2O_4$ $[M+H]^+$: 577.4938; found: 577.4938.

3,4-[Bis-(*S*)-3,7-dimethyloctyloxy]-5-octyloxybenzoylaminoethylamide (3g): Light yellow waxy material (67%); ^{1}H NMR (400 MHz, $CDCl_3$, TMS, 300 K): $\delta = 6.98$ (s, 2H), 4.01–3.97 (m, 6H), 3.48–3.46 (m, 2H), 2.95 (m, 2H), 1.71–1.12 (m, 32H), 0.96–0.85 ppm (m, 21H); UV/Vis (CH_2Cl_2): λ_{max} (ε) = 295 (3100), 264 nm (9510 $M^{-1}cm^{-1}$); HRMS (ESI): *m/z* calcd for $C_{37}H_{69}N_2O_4$ $[M+H]^+$: 605.5252; found: 605.5252.

***N,N'*-Di(3,4,5-trioctyloxybenzoylaminoethyl)perylene-3,4:9,10-tetracarboxylic acid bisimide (PBI-2)**: Compound **3b** (0.40 g, 0.73 mmol), perylene tetracarboxylic acid bisanhydride (0.136 g), $Zn(OAc)_2$ (0.139 g), and imidazole (10.5 g) were taken together in a flask and were stirred at 130°C for 24 h under an argon atmosphere. The reaction mixture was cooled to room temperature and poured into methanol (100 mL). The red precipitate was filtered and the solid was washed several times with methanol. The crude product was purified by using column chromatography with silica gel as the stationary phase and 5% MeOH in $CHCl_3$ as the eluent. The pure product was obtained as a bright red powder (35%). M.p. 258–260°C; ^{1}H NMR (400 MHz, $CDCl_3$, TMS, 300 K): $\delta =$ 8.50 (d, $J = 7.6$ Hz, 4H), 8.36 (d, $J = 8.0$ Hz, 4H), 7.08 (s, 2H), 7.00 (s, 4H), 4.53 (m, 4H), 3.98 (m, 12H), 3.88 (m, 4H), 1.80–1.15 (m, 72H), 0.88 ppm (m, 18H); UV/Vis ($CHCl_3$): λ_{max} (ε) = 528 (79100), 491 (48300), 460 nm (17900 $M^{-1}cm^{-1}$); HRMS (ESI): *m/z* calcd for $C_{90}H_{125}N_4O_{12}$ $[M+H]^+$: 1453.9288; found: 1453.9285.

All other PBI gelators were made by following the above procedure.

***N,N'*-Di[3,4,5-(tris-4-methylbutyloxy)benzoylaminoethyl]perylene-3,4:9,10-tetracarboxylic acid bisimide (PBI-4)**: Yield: 49%; m.p. 285–287°C; ^{1}H NMR (400 MHz, $CDCl_3$, TMS, 300 K): $\delta = 8.66$ (d, $J = 8.0$ Hz, 4H), 8.58 (d, $J = 8.04$ Hz, 4H), 7.25 (along with residual solvent peak), 6.98 (s, 4H), 4.56 (m, 4H), 4.06–3.96 (m, 16H), 1.72–1.60 (m, 16H), 0.97–0.92 ppm (m, 36H); UV/Vis ($CHCl_3$): λ_{max} (ε) = 528 (80200), 491 (51100), 460 nm (18100 $M^{-1}cm^{-1}$); HRMS (ESI): *m/z* calcd for $C_{72}H_{88}N_4NaO_{12}$ $[M+Na]^+$: 1223.6291; found: 1223.6290.

***N,N'*-Di[3,4,5-(tris-2-ethylhexyloxy)benzoylaminoethyl]perylene-3,4:9,10-tetracarboxylic acid bisimide (PBI-5)**: Yield: 54%; m.p. 215–217°C; ^{1}H NMR (400 MHz, $CDCl_3$, TMS, 300 K): $\delta = 8.56$ (d, $J = 7.6$ Hz, 4H), 8.43 (d, $J = 8.1$ Hz, 4H), 7.05 (t, 2H), 7.00 (s, 4H), 4.55 (m, 4H), 3.89–3.82 (m, 16H), 1.76–1.28 (m, 54H), 0.90 ppm (m, 36H); UV/Vis ($CHCl_3$): λ_{max} (ε) = 528 (81300), 491 (51400), 460 nm (19100 $M^{-1}cm^{-1}$); HRMS (ESI): *m/z* calcd for $C_{90}H_{124}N_4NaO_{12}$ $[M+Na]^+$: 1475.9108; found: 1475.9108.

***N,N'*-Di{4-[(*S*)-3,7-dimethyloctyloxy-3,5-dioctyloxy]benzoylaminoethyl}-perylene-3,4:9,10-tetracarboxylic acid bisimide (PBI-6)**: Yield: 48%; m.p. 251–254°C; ^{1}H NMR (400 MHz, $CDCl_3$, TMS, 300 K): $\delta = 8.57$ (d, 4H, $J = 7.7$ Hz), 8.47 (d, 4H, $J = 8.0$ Hz), 7.02 (t, 2H), 6.98 (s, 4H), 4.55 (m, 4H), 3.01–3.87 (m, 16H), 1.82–0.84 ppm (m, 60H); UV/Vis ($CHCl_3$): λ_{max} (ε) = 528 (80400), 491 (50000), 460 nm (18000 $M^{-1}cm^{-1}$); HRMS (ESI): *m/z* calcd for $C_{94}H_{133}N_4O_{12}$ $[M+H]^+$: 1509.9914; found: 1509.9909.

***N,N'*-Di{3,4-bis-[(*S*)-3,7-dimethyloctyloxy-5-octyloxy]benzoylaminoethyl}-perylene-3,4:9,10-tetracarboxylic acid bisimide (PBI-7)**: Yield: 50%; m.p. 218–220°C; ^{1}H NMR (400 MHz, $CDCl_3$, TMS, 300 K): $\delta = 8.56$ (d, $J =$ 7.7 Hz, 4H), 8.44 (d, $J = 8.0$ Hz, 4H), 7.00 (t, 2H), 6.94 (s, 4H), 4.49 (m, 4H), 3.01–3.82 (m, 16H), 1.81–0.83 ppm (m, 68H); UV/Vis ($CHCl_3$): λ_{max} (ε) = 528 (81700), 491 (51200), 460 nm (18500 $M^{-1}cm^{-1}$); HRMS (ESI): *m/z* calcd for $C_{98}H_{140}N_4NaO_{12}$ $[M+H]^+$: 1566.0148; found: 1566.0344.

Acknowledgements

Financial support by DFG for the research training school GRK 1221 "Control of electronic properties of aggregated π-conjugated molecules" is gratefully acknowledged. S.G. thanks the Alexander von Humboldt Foundation for a postdoctoral fellowship.

[1] a) J.-M. Lehn, *Supramolecular Chemistry—Concepts and Perspectives*, Wiley-VCH, Weinheim (Germany), **1995**; b) G. M. Whitesides, J. P. Mathias, C. T. Seto, *Science* **1991**, *254*, 1312; c) J.-M. Lehn, *Proc. Natl. Acad. Sci. USA* **2002**, *99*, 4763.

[2] a) G. H. Brown, J. J. Wolken, *Liquid Crystals and Biological Structures*, Academic Press, New York (USA), **1979**; b) G. M. Whitesides, B, Grzybowski, *Science* **2002**, *295*, 2418; c) H. Ringsdorf, B. Schlarb, J. Venzmer, *Angew. Chem.* **1988**, *100*, 117; *Angew. Chem. Int. Ed. Engl.* **1988**, *27*, 113.

[3] a) F. M. Hoeben, P. Jonkheijm, E. W. Meijer, A. P. H. J. Schenning, *Chem. Rev.* **2005**, *105*, 1491; b) *Supramolecular Dye Chemistry, Topics in Current Chemistry, Vol. 258* (Ed.: F. Würthner), Springer, Berlin (Germany), **2005**.

[4] a) W. Pisula, M. Kastler, D. Wasserfallen, J. W. F. Robertson, F. Nolde, C. Kohl, K. Müllen, *Angew. Chem.* **2006**, *118*, 834; *Angew. Chem. Int. Ed.* **2006**, *45*, 819; b) J. P. Hill, W. Jin, A. Kosaka, T. Fukushima, H. Ichihara, T. Shimomura, K. Ito, T. Hashi-zume, N. Ishii, T. Aida, *Science* **2004**, *304*, 1481; c) T. van der Boom, R. T. Hayes, Y. Zhao, P. Bushard, E. A. Weiss, M. R. Wasielewski, *J. Am. Chem. Soc.* **2002**, *124*, 9582; d) F. Würthner, Z. Chen, F. J. M. Hoeben, P. Osswald, C.-C. You, P. Jonkheijm, J. von Herrikhuyzen, A. P. H. J. Schenning, P. P. A. M. van der Schoot, E. W. Meijer, E. H. A. Beckers, S. C. J. Meskers, R. A. J. Janssen, *J. Am. Chem. Soc.* **2004**, *126*, 10611; e) M. G. Debije, Z. Chen, J. Piris, R. B. Neder, M. M. Watson, K. Müllen, F. Würthner, *J. Mater. Chem.* **2005**, *15*, 1270; f) S. Sergeyev, W. Pisulab, Y. H. Geerts, *Chem. Soc. Rev.* **2007**, *36*, 1902; g) A. Ajayaghosh, P. Chithra, R. Varghese, *Angew. Chem.* **2007**, *119*, 234; *Angew. Chem. Int. Ed.* **2007**, *46*, 230; h) A. Ajayaghosh, P. Chithra, R. Varghese, K. P. Divya, *Chem. Commun.* **2008**, 969; i) J. Puigmartí-Luis, V. Laukhin, Á. Pérez del Pino, J. Vidal-Gancedo, C. Rovira, E. Laukhina, D. B. Amabilino, *Angew. Chem.* **2007**, *119*, 242; *Angew. Chem. Int. Ed.* **2007**, *46*, 238; j) T. Akutagawa, K. Kakiuchi, T. Hasegawa, S. Noro, T. Nakamura, H. Hasegawa, S. Mashiko, J. Becher, *Angew. Chem.* **2005**, *117*, 7449; *Angew. Chem. Int. Ed.* **2005**, *44*, 7283.

[5] a) J. van Esch, F. Schoonbeek, M. De Loos, H. Kooijman, E. M. Veen, R. M. Kellogg, B. L. Feringa, *Supramolecular Science: Where It Is and Where It Is Going* (Eds.: R. Ungaro, E. Dalcanale), Kluwar, The Netherlands, **1999**, p. 233; b) R. E. Melendez, A. J. Carr, B. R. Linton, A. D. Hamilton, *Struct. Bonding (Berlin)* **2000**, 31; c) U. Beginn, *Prog. Polym. Sci.* **2003**, *28*, 1049; d) *Low Molecular Mass Gelators (Topics in Current Chemistry), Vol. 256* (Ed.: F. Fages), Springer, Berlin (Germany), **2005**; e) H. Bouas-Laurent, J.-P. Desvergne, *Molecular Gels: Materials with Self-Assembled Fibrillar Networks* (Eds.: R. G. Weiss, P. Terech), Springer, Netherlands, **2006**, Chapter 12.

[6] a) S.-i. Tamaru, M. Nakamura, M, Takeuchi, S. Shinkai, *Org. Lett.* **2001**, *3*, 3631; b) M. Shirakawa, S.-i. Kawano, N. Fujita, K. Sada, S. Shinkai, *J. Org. Chem.* **2003**, *68*, 5037; c) S. Malik, S. Kawano, N. Fujita, S. Shinkai, *Tetrahedron* **2007**, *63*, 7326.

[7] H. Engelkamp, S. Middelbeek, R. J. M. Nolte, *Science* **1999**, *284*, 785.

[8] a) A. Ajayaghosh, V. K. Praveen, *Acc. Chem. Res.* **2007**, *40*, 644; b) A. Ajayaghosh, V. K. Praveen, C. Vijayakumar, S. J. George, *Angew. Chem.* **2007**, *119*, 6376; *Angew. Chem. Int. Ed.* **2007**, *46*, 6260; c) A. Ajayaghosh, C. Vijayakumar, R. Varghese, S. J. George, *Angew. Chem.* **2006**, *118*, 470; *Angew. Chem. Int. Ed.* **2006**, *45*, 456; d) A. Ajayaghosh, S. J. George, *J. Am. Chem. Soc.* **2001**, *123*, 5148; e) A. Ajayaghosh, R. Varghese, V. K. Praveen, S. Mahesh, *Angew. Chem.* **2006**, *118*, 3339; *Angew. Chem. Int. Ed.* **2006**, *45*, 3261; f) A. Ajayaghosh, R. Varghese, S. Mahesh, V. K. Praveen, *Angew. Chem.* **2006**, *118*, 7893; *Angew. Chem. Int. Ed.* **2006**, *45*, 7729.

[9] a) F. S. Schoonbeek, J. H. Van Esch, B. Wegewijs, D. B. A. Rep, M. P. De Haas, T. M. Klapwijk, R. M. Kellogg, B. L. Feringa, *Angew. Chem.* **1999**, *111*, 1486; *Angew. Chem. Int. Ed.* **1999**, *38*, 1393; b) S. Kawano, N. Fujita, S. Shinkai, *Chem. Eur. J.* **2005**, *11*, 4735.

[10] a) K. Sugiyasu, N. Fujita, S. Shinkai, *Angew. Chem.* **2004**, *116*, 1249; *Angew. Chem. Int. Ed.* **2004**, *43*, 1229; b) F. Würthner, B. Hanke, M. Lysetska, G. Lambright, G. S. Harms, *Org. Lett.* **2005**, *7*, 967; c) S. Yagai, Y. Monma, N. Kawauchi, T. Karatsu, A. Kitamura, *Org. Lett.* **2007**, *9*, 1137.

[11] C. W. Struijik, A. B. Sieval, J. E. J. Dakhorst, M. Dijk, P. Kimkes, R. B. M. Koehorst, H. Donker, T. J. Schaafsma, S. J. Picken, A. M. van de Craats, J. M. Warman, H. Zuilhof, E. J. R. Sudhölter, *J. Am. Chem. Soc.* **2000**, *122*, 11057.

[12] H. Langhals, J. Karolin, L. B. Johansson, *J. Chem. Soc. Faraday Trans.* **1998**, *94*, 2919.

[13] a) F. Würthner, *Chem. Commun.* **2004**, 1564; b) F. Würthner, *Pure Appl. Chem.* **2006**, *78*, 2341.

[14] a) F. C. DeSchryver, T. Vosch, M. Cotlet, M. van der Auweraer, K. Müllen, J. Hofkens, *Acc. Chem. Res.* **2005**, *38*, 514; b) A. Sautter, B. K. Kaletas, D. G. Schimd, R. Dobrawa, M. Zimine, G. Jung, I. H. M. Van Stokkum, L. De Cola, R. M. Williams, F. Würthner, *J. Am. Chem. Soc.* **2005**, *127*, 6719.

[15] a) M. P. O'Neil, M. P. Niemczyk, W. A. Svec, D. Gosztola, G. L. Gaines III, M. R. Wasielewski, *Science* **1992**, *257*, 63; b) E. H. A. Beckers, S. C. J. Meskers, A. P. H. J. Schenning, Z. Chen, F. Würthner, R. A. J. Jansses, *J. Phys. Chem. A* **2005**, *108*, 6933; c) A. Prodi, C. Chiorboli, F. Scandola, E. Iengo, E. Alessio, R. Dobrawa, F. Würthner, *J. Am. Chem. Soc.* **2005**, *127*, 1454; d) M. S. Rodriguez-Morgade, T. Torres, C. Atienza-Castellanos, D. M. Guldi, *J. Am. Chem. Soc.* **2006**, *128*, 15145.

[16] a) A. Kraft, A. C. Grimsdale, A. B. Holmes, *Angew. Chem.* **1998**, *110*, 416; *Angew. Chem. Int. Ed.* **1998**, *37*, 402; b) C. Karapire, C. Zafer, S. Icli, *Synth. Met.* **2004**, *145*, 51.

[17] a) C. D. Dimitrakopoulos, P. R. L. Malenfant, *Adv. Mater.* **2002**, *14*, 99; b) B. A. Jones, M. J. Ahrens, M.-H. Yoon, A. Facchetti, T. J. Marks, M. R. Wasielewski, *Angew. Chem.* **2004**, *116*, 6523; *Angew. Chem. Int. Ed.* **2004**, *43*, 6363; c) F. Würthner, R. Schmidt, *ChemPhysChem* **2006**, *7*, 793; d) J. Hak Oh, S. Liu, Z. Bao, R. Schmidt, F. Würthner, *Appl. Phys. Lett.* **2007**, *91*, 212107; e) R. Schmidt, M. M. Ling, J. H. Oh, M. Winkler, M. Könemann, Z. Bao, F. Würthner, *Adv. Mater.* **2007**, *19*, 3692; f) P. R. L. Malenfant, C. D. Dimitrakopoulos, J. D. Gelorme, L. L. Kosar, T. O. Graham, *Appl. Phys. Lett.* **2002**, 2517.

[18] a) C. W. Tang, *Appl. Phys. Lett.* **1986**, *48*, 183; b) L. Schmidt-Mende, A. Fechtenkötter, K. Müllen, E. Moons, R. H. Friend, J. D. MacKenzie, *Science* **2001**, *293*, 1119.

[19] a) A. Syamakumari, A. P. H. J. Schenning, E. W. Meijer, *Chem. Eur. J.* **2002**, *8*, 3353; b) J. van Herrikhuyzen, A. Syamakumari, A. P. H. J. Schenning, E. W. Meijer, *J. Am. Chem. Soc.* **2004**, *126*, 10021; c) K. Balakrishnan, A. Datar, T. Naddo, J. Huang, R. Oitker, M. Yen, J. Zhao, L. Zang, *J. Am. Chem. Soc.* **2006**, *128*, 7390; d) T. van der Boom, R. T. Hayes, Y. Zhao, P. J. Bushard, E. A. Weiss, M. R. Wasielewski, *J. Am. Chem. Soc.* **2002**, *124*, 9582; e) W. Wang, L. S. Li, G. Helms, H. H. Zhou, A. D. Q. Li, *J. Am. Chem. Soc.* **2003**, *125*, 1120; f) W. Wang, W. Wan, H.-H. Zhou, S. Q. Niu, A. D. Q. Li, *J. Am. Chem. Soc.* **2003**, *125*, 5248; g) A. D. Q. Li, W. Wang, L. Q. Wang, *Chem. Eur. J.* **2003**, *9*, 4594; h) S. M. Lindner, S. Hüttner, A. Chiche, M. Thelakkat, G. Krausch, *Angew. Chem.* **2006**, *118*, 3442; *Angew. Chem. Int. Ed.* **2006**, *45*, 3364; i) F. Würthner, C. Thalacker, A, Sautter, W. Schartl, W, Ibach, O. Hollricher, *Chem. Eur. J.* **2000**, *6*, 3871; j) R. P. Sijbesma, E. W. Meijer, *Chem. Commun.* **2003**, 5; k) C. Thalacker, F. Würthner, *Adv. Funct. Mater.* **2002**, *12*, 209; l) A. P. H. J. Schenning, J. von Herrikhuyzen, P. Jonkheijm, Z. Chen, F. Würthner, E. W. Meijer, *J. Am. Chem. Soc.* **2002**, *124*, 10252; m) B. Jancy, S. K. Asha, *Chem. Mater.* **2008**, *20*, 169.

[20] a) Z. Chen, V. Stepanenko, V. Dehm, P. Prins, L. D. A. Siebbeles, J. Seibt, P. Marquetand, V. Engel, F. Würthner, *Chem. Eur. J.* **2007**, *13*, 43; b) F. Würthner, Z. Chen, V. Dehm, V. Stepanenko, *Chem. Commun.* **2006**, 1188.

[21] X.-Q. Li, V. Stepanenko, Z. Chen, P. Prins, L. D. A. Siebbeles, F. Würthner, *Chem. Commun.* **2006**, 3871.

[22] A. Brizard, R. Oda, I. Huc, *Top. Curr. Chem.* **2005**, *256*, 167.

[23] F. Würthner, C. Bauer, V. Stepanenko, S. Yagai, *Adv. Mater.* **2008**, *20*, 1695.

[24] a) A. Wu, L. Isaacs, *J. Am. Chem. Soc.* **2003**, *125*, 4831; b) P. Mukhopadhyay, P. Y. Zavalij, L. Isaacs, *J. Am. Chem. Soc.* **2006**, *128*, 14093; c) K. Sugiyasu, S-i. Kawano, N. Fujita, S. Shinkai, *Chem. Mater.* **2008**, *20*, 2863.

[25] Remarkably similar structures have been obtained from very different building block, see: L.-s. Li, H. Jiang, B. W. Messmore, S. R. Bull, S. Stupp, *Angew. Chem.* **2007**, *119*, 5977; *Angew. Chem. Int. Ed.* **2007**, *46*, 5873.

[26] For a recent review on chiral supramolecular aggregates, see: A. R. A. Palmans, E. W. Meijer, *Angew. Chem.* **2007**, *119*, 9106; *Angew. Chem. Int. Ed.* **2007**, *46*, 8948.

[27] Even at a 20% incorporation of the chiral **PBI-3** in a H-type stack of achiral **PBI-1**, the CD signal intensity is almost saturated due to the "sergeant-and-soldier" principle. For few recent examples on such chiral amplifications in other supramolecular assemblies, see:

a) A. Lohr, F. Würthner, *Chem. Commun.* **2008**, 2227; b) A. J. Wilson, J. Van Gestel, R. P. Sijbesma, E. W. Meijer, *Chem. Commun.* **2006**, 4404; c) S. R. Nam, H. Y. Lee, J.-I. Hong, *Chem. Eur. J.* **2008**, *14*, 6040.

[28] a) H. V. Berlepsch, S. Kirstein, C. Böttcher, *J. Phys. Chem. B* **2003**, *107*, 9646; b) J. Aimi, Y. Ngamine, A. Tsuda, A. Muranaka, M. Uchiyama, T. Aida, *Angew. Chem.* **2008**, *120*, 5231; *Angew. Chem. Int. Ed.* **2008**, *47*, 5153; c) Y. Zhang, P. Chen, M. Liu, *Chem. Eur. J.* **2008**, *14*, 1793.

[29] Although CD spectroscopic studies revealed a preferential population of one-handed helices in chiral solvent, AFM images of the gels made in (*R*)-limonene were found to consist of both types of helices. It should be noted that gelation is a very fast process, which occurs at a much higher chromophore concentration than the solution chiroptical studies. Thus, the chiral induction from external sources may not be adequate in effectively populating only one-handed helices. Even **PBI-6**, which has one chiral alkyl group as a peripheral substituent, forms both handed helices, which indicates a weak influence of the remote chiral center in the alkyl side chain on the chromophore packing in the fast gelation process. However, in **PBI-3**, in which all of the three alkyl substituents are chiral, only *P*-type helices were found in AFM studies.

[30] a) A. Tsuda, Md. A. Alam, T. Harada, T. Yamaguchi, N. Ishii, T. Aida, *Angew. Chem.* **2007**, *119*, 8346; *Angew. Chem. Int. Ed.* **2007**, *46*, 8198; b) M. Wolffs, S. J. George, Ž. Tomović, S. C. J. Meskers, A. P. H. J. Schenning, E. W. Meijer, *Angew. Chem.* **2007**, *119*, 8351; *Angew. Chem. Int. Ed.* **2007**, *46*, 8203; c) G. P. Spada, *Angew. Chem.* **2008**, *120*, 646; *Angew. Chem. Int. Ed.* **2008**, *47*, 636; d) J. M. Ribó, J. Crusats, F. Sagues, J. M. Claret, R. Ruvires, *Science* **2001**, *292*, 2063.

[31] For J-type π stacking of PBI dyes in the solid state, see: a) F. Graser, E. Hädicke, *Liebigs Ann. Chem.* **1984**, 483; b) G. Klebe, F. Graser, E. Hädicke, J. Berndt, *Acta Crystallogr. Sect. A* **1989**, *45*, 69; c) J. Mizuguchi, *J. Appl. Phys.* **1998**, *84*, 4479.

[32] For recent examples of J-aggregating PBI chromophores, see: a) T. E. Kaiser, H. Wang, V. Stepanenko, F. Würthner, *Angew. Chem.* **2007**, *119*, 5637; *Angew. Chem. Int. Ed.* **2007**, *46*, 5541; b) S. Yagai, T. Seki, T. Karatsu, A. Kitamura, F. Würthner, *Angew. Chem.* **2008**, *120*, 3415; *Angew. Chem. Int. Ed.* **2008**, *47*, 3367.

[33] R. F. Ludlow, S. Otto, *Chem. Soc. Rev.* **2008**, *37*, 101–108.

[34] A. Wicklein, S. Ghosh, F. Würthner, M. Thelakkat, unpublished results.

[35] D. D. Perrin, W. L. F. Armarego, D. R. Perrin, *Purification of Laboratory Chemicals*, 2nd ed., Pergamon, Oxford, **1980**.

Received: July 18, 2008
Published online: November 13, 2008

